AD-A150 725 OBSERVATION OF PURE RESONANCE AND THRESHOLD EFFECTS IN ELECTRON IMPACT EX..(U) UNIVERSITY OF SOUTHERN CALIFORNIA LOS ANGELES DEPT OF CHEMIST.. 1/1

UNCLASSIFIED R MCADAMS ET AL. DEC 84 N00014-82-K-0330 F/G 20/8 NL

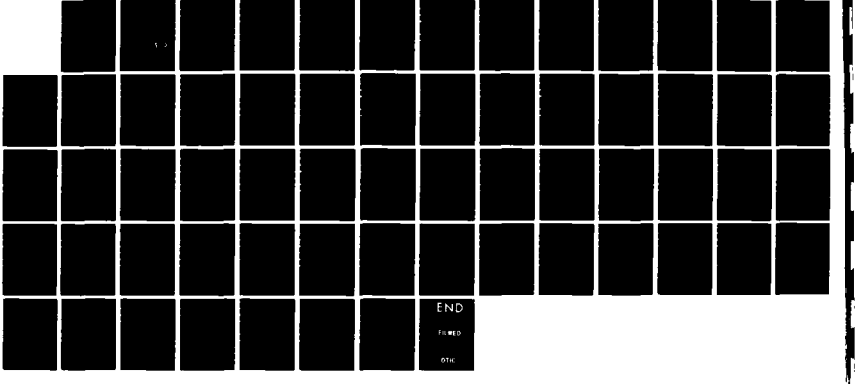

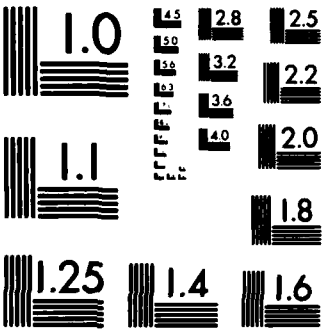

Unclassified

SECURITY CLASSIFICATION OF THIS PAGE (When Data Entered)

(2)

REPORT DOCUMENTATION PAGE	READ INSTRUCTIONS BEFORE COMPLETING FORM
1 REPORT NUMBER: 412:KFM:tfe	2 GOVT ACCESSION NO. / 3 RECIPIENT'S CATALOG NUMBER
4 TITLE (and Subtitle): OBSERVATION OF PURE RESONANCE AND THRESHOLD EFFECTS IN ELECTRON IMPACT EXPERIMENTS IN HIGH INTENSITY LASER FIELDS	5 TYPE OF REPORT & PERIOD COVERED: FINAL REPORT 4/1/82 - 9/30/84
	6 PERFORMING ORG. REPORT NUMBER: N000014-82-K-0330
7 AUTHOR(s): R. McAdams, H.S. Taylor, S. Trajmar	8 CONTRACT OR GRANT NUMBER(s): N000014-82-K-0330
9 PERFORMING ORGANIZATION NAME AND ADDRESS: Department of Chemistry, University of Southern California, Los Angeles, CA 90089-0482	10 PROGRAM ELEMENT, PROJECT, TASK AREA & WORK UNIT NUMBERS
11 CONTROLLING OFFICE NAME AND ADDRESS: Clinton R. Kerner, dministrative Contracting Officer, ONR, asadena, CA 91106	12 REPORT DATE: December 1984
	13 NUMBER OF PAGES: 32 pages + figures
MONITORING AGENCY NAME & ADDRESS (if different from Controlling Office)	15 SECURITY CLASS. (of this report): unclassified
	15a DECLASSIFICATION/DOWNGRADING SCHEDULE

DISTRIBUTION STATEMENT (of this Report)

DISTRIBUTION STATEMENT A
Approved for public release;
Distribution Unlimited

DISTRIBUTION STATEMENT (of the abstract entered in Block 20, if different from Report)

18 SUPPLEMENTARY NOTES

DTIC ELECTE FEB 28 1985 S D B

19 KEY WORDS (Continue on reverse side if necessary and identify by block number)

20 ABSTRACT (Continue on reverse side if necessary and identify by block number)

see attached

DD FORM 1 JAN 73 1473 EDITION OF 1 NOV 65 IS OBSOLETE

unclassified

SECURITY CLASSIFICATION OF THIS PAGE (When Data Entered)

AD-A150 725

DTIC FILE COPY

85 02 04 031

Electron-Atom Scattering in a Radiation Field

R. McAdams

H. S. Taylor

S. Trajmar

University of Southern California
Los Angeles, California

ABSTRACT

This report describes experiments which were aimed to: 1) observe induced one photon free-free transitions associated with electron scattering by rare gas atoms in a CO_2 laser field; 2) observe resonances in the free-free channel under experimental conditions when direct scattering is eliminated (by making the electric polarization vector and the momentum transfer vector perpendicular to each other).

We have detected free-free transtions associated with elastic scattering by Ar and Xe at 141° and 90° scattering angles, respectively, using incident electron energies near resonances. Resonances in the elastic channel were readily observed for He, Ar and Xe but due to poor statistics, we were not able to demonstrate the resonances in the free-free channels. There was indication, however, that (in agreement with the soft photon approximation) the free-free direct scattering amplitude was zero when the laser polarization direction was perpendicular to the momentum transfer direction.

On the basis of our studies, it was conlcuded, that (although the aims described above could be achieved with our apparatus) it would require much more time, than presently is available to us, to demonstrate the effects with proper signal to noise conditions.

TABLE OF CONTENTS

1. INTRODUCTION

Over the past few years, in the field of atomic collisions, great interest has been shown in how the collision processes may be modified by the presence of a radiation field. The research described in this report deals specifically with electron-atom scattering in a laser field. While undergoing scattering from the potential due to its interaction with the atom, the electron can emit or absorb an integral number of photons of the laser wavelength. Since the electron must then change its energy and momentum but still remains unbound to the atom it is said to undergo a free-free transition. In accordance with the laws of conservation of energy and momentum the emission or absorption of radiation must take place in the presence of a third body (the atom or a molecule or an ion). The process may be written as

$$e^-(E_i) + A + \text{laser field} \rightarrow e^-(E_i \pm N\,\hbar\omega) + A + \text{laser field}$$

where E_i is the incident energy of the electron, N is the number of photons absorbed or emitted in the collision, ω is the laser frequency and $\hbar$ is Plancks constant.

Free-free transitions are of interest from both a practical and academic standpoint. The infra-red opacity of the solar atmosphere is due to these transitions; they are a mechanism for laser heating of a plasma when the free electrons absorb incident radiation, when a laser is focussed into a gas it may multiphoton ionize the atoms and the photoelectrons continue to absorb photons raising their kinetic energy above the ionization potential of surrounding neutral atoms and hence causing collisional ionization and breakdown of the gas.

Until recently information on free-free transitionss had to be derived from bulk plasma properties. However, in order to compare theoretical descriptions

of the process with experimental results it is necessary to carry out the experiments at a level where averages over unmeasured parameters are minimized. In the present study we have developed a crossed beam apparatus to observe free-free transitions where all experimental parameters are known. Some previous crossed beam experiments have been carried out in the past[1-3] and these will be alluded to briefly in the next section. Their purpose was to test theoretical models of the collisions. In these experiments measured differential cross sections for the emission or absorption of a given number of photons are compared with theoretical ones.

A consequence of a theoretical model (known as the soft photon limit) is the prediction of a rather unique effect. It indicates that, with the correct choice of completely controlable electron kinematical vectors and the laser polarization it is possible to separate the direct and resonant scattering amplitudes associated with free-free transitions. Thus, instead of observing a resonance through the interference between direct and resonant amplitudes, it would be possible to observe the purely resonant effect. This observation would greatly enhance our understanding the resonances.

The purpose of this research is to test this theoretical prediction. Only one previous experiment observed electron-atom resonances in the free-free cross section, however, at that time the theory of the effect had not been developed and also the laser in that case was not polarized and therefore the prediction could not be tested. In the next section of the report we will describe the basic results of the theoretical description and show how it might be possible to separate the direct and the resonant contributions to the scattering cross section. In subsequent sections we will summarize our approach to the experiment and then go on to describe the apparatus and give the results of our experiments.

2. THEORETICAL BACKGROUND

2.1 Theory of free-free transitions - direct scattering

Consider, as shown schematically in Figure 2.1, an electron of energy E, incident upon an atom while the system is being irradiated by an electromagnetic wave. The electron is scattered through an angle θ due to its interaction with the atomic electrons. If the e.m. field was absent the process would be described by a scattering amplitude $f(\theta)$. The differential cross section for the scattering $d\sigma/d\Omega$, is proportional to $|f(\theta)|^2$. We shall only consider elastic scattering in this discussion. As described in the previous section the introduction of an electromagnetic field can stimulate the scattering electron to emit or absorb photons of the laser wavelength.

In order to describe this process Kroll and Watson[1] carried out a perturbation expansion. The laser field was treated as a plane wave given by the vector potential

$$\bar{A} = A_o \hat{\epsilon} \cos \omega t \qquad (1)$$

where A_o is the amplitude of the potential, $\hat{\epsilon}$ is the laser polarization vector and ω is the laser frequency. They used the dimensionless parameter $\hbar\omega/E$ to make the expansion and retained only the first two terms in the expansion. Their result for the differential cross section for the absorption or emission of N photons during the scattering process can be expressed as

$$\frac{d\sigma_{ff}}{d\Omega}^{(N)} = \frac{k_f}{k_i} J_N^2(2\Gamma) \frac{d\sigma}{d\Omega} \qquad (2)$$

where $k_{f,i}$ is the final or incident electron momentum, $d\sigma/d\Omega$ is the elastic scattering cross section in the absence of the laser, J_N is a Bessel function of

order N, and Γ is a parameter given by

$$\Gamma^2 = 4.86 \times 10^{-13} \lambda^4 F E_i \left[\frac{\hat{\varepsilon} \cdot \bar{Q}}{2k_i}\right] \qquad (3)$$

where λ is the laser wavelength in microns, F is the flux density in watts/cm^2 and $\bar{Q}$ is the momentum transfer vector ($\hat{Q}$ is the unit vector in the direction of $\bar{Q}$).

At this stage a number of comments should be made about Eq. 2. Its derivation dependend on $\hbar\omega/E \ll 1$. This is known as the soft photon approximation $\hbar\omega/E_i$ can be looked upon as the ratio of the collision duration ($\sim \hbar/E$) to the aprroximate time for a photon to be absorbed or emitted ($1/\omega$). If this ratio is small then the photon absorption or emission does not take place during the collision. Thus we have the somewhat remarkable result that the differential cross section for a N photon transition factors into the product of two terms; the Bessel function describes the electron-laser interaction and $d\sigma/d\Omega$ gives the actual scattering cross section for the electron whose wavefunction is modified by the laser.

Equation 2 has a number of important consequences. Firstly, it shows a strong (4th power) dependence of laser wavelength - hence, it is more useful to use long wavelength lasers such as the CO_2 laser at 10.6 μm to observe the effect. Secondly, the only dependence of the cross section of the target used is through the elastic cross section factor. This means that it is better to use targets such as the heavy rare gase atoms which have relatively large elastic scattering cross sections. As shown by Mittleman,[2] Eq. 2 should be valid for laser power densities of up to 10^{12} W cms^{-2}.

If one sums the free-free cross section over all photon transitions a sum rule is obtained

$$\sum_{N=-\infty}^{+\infty} \frac{d\sigma_{ff}}{d\Omega}^{(N)} = \frac{d\sigma}{d\Omega} \qquad (4)$$

Thus the individual contributions must total the cross section without the laser.

An alternative approach to derive the free-free cross section has been made by Kruger and Schulz.[3] Again they used a perturbation method but expanded in terms of the laser power density. Thus it should only be valid for single photon transitions and also at low power density. Their result for the differential free-free cross section for a single photon transition, in the soft photon limit i.e. $\hbar\omega \to 0$, is

$$\frac{d\sigma_{ff}^{(1)}}{d\Omega} = \frac{k_f}{k_i} \Gamma^2 \frac{d\sigma}{d\Omega} \qquad (5)$$

This result can be derived from that of Kroll and Watson using the following relationship for Bessel functions of small argument

$$J_N(\chi) \to (\chi/2)^N$$

Because of the power limitations of the laser used in this our study Eq. 5 is more appropriate to use than Eq. 2.

Substituting for Γ^2 in Eq. 5 and using $\lambda = 10.6$ μm we obtain

$$\frac{d\sigma_{ff}}{d\Omega} = 6.13 \times 10^{-9} E_i F \sin^2 \theta/2 \cos^2 \alpha \frac{d\sigma}{d\Omega} \qquad (6)$$

where θ is the scattering angle and α is the angle between the laser polarization and the momentum transfer direction. It can be seen immediately that the ratio of the free-free to the elastic scattering cross section is

largest at high energies and large scattering angles i.e. under large momentum transfer conditions.

2.2 Theory of free-free transitions - resonance scattering

Resonances in electron-atom scattering cross sections have been known for about twenty years and they have aroused considerable theoretical and experimental interest. Some attention recently has also been paid to the effect of resonances on free-free cross sections. We will now look at the predictions made for resonant scattering within the soft photon approximation.

Consider the occurrance of a resonance at an energy E_R in the elastic scattering cross section. It was Kruger and Schulz[3] who first pointed out that in the free-free cross section for, say, one photon absorption two resonances will be observed. These resonances will occur at incident energies of $E_i = E_R$ and $E_i = E_R - \hbar\omega$. Although this latter energy is not the resonant one, excitation of the resonance takes place by the electron increasing its energy by that of one photon which then puts it on resonance. At the former energy, resonance excitation takes place and then the photon is absorbed. In both cases the final energy of the electron is increased by that of a photon.

At the resonance energy there is never purely resonant scattering. There exists a direct scattering amplitude as well. Since there are then two paths to the same final state, interference takes place and experimentally this is observed as the so-called Fano profile in the scattering intensity vs. E_i curve . If the direct scattering amplitude was zero then the resonance would be observed as a pure Breit-Wigner profile. In such a case it would obviously be easier to obtain the resonance parameters such as position and width. Jung and Taylor[4] have shown that within the soft photon approximation there is the possibility of separating the direct and resonance amplitudes. More explicitly the direct amplitude can be completely suppressed leaving only the resonant

one.

In order to see how this might be accomplished we rewrite the soft photon approximation to the scattering amplitude for an N photon transition as

$$f_N(E_i,\theta) = \sum_R J_{N-R}\,(\bar{\alpha}.\bar{k}_f)\; f(E_i + k\omega,\theta)\; J_k\,(-\bar{\alpha}.\bar{k}_i) \qquad (7)$$

where $\bar{\alpha} = e\,A_o\,\hat{\epsilon}/mc\omega$ and we have set $\hbar = 1$. This is a generalized version of the soft photon approximation given earlier. The transition can be thought of as proceeding through the following steps which correspond to the three factors on the right hand side of Eq. 7. Starting from the right to left of Eq. 7 we have:

(i) the term $J_k(-\bar{\alpha}.\bar{k}_i)$ represents the absorption or emission of k photons from the laser field by the incident electron,

(ii) the soft photon approximation is based upon the electron-laser interaction taking place well away from the scattering region and the elastic scattering is then described by the scattering amplitude $f(E_i \pm k\omega,\theta)$ and

(iii) finally, the scattered electron undergoes further interaction with the laser emitting or absorbing N-k photons to give the final electron state according to an N-photon transition.

These processes are summed over all possible values of k. Suppose that there is a resonance in the cross section and we then decompose the scattering amplitude into a resonance part and a direct scattering part, i.e.

$$f(E_i + k\omega,\theta) = f^R(E_i \pm k\omega,\theta) + f^o(E_i \pm k\omega,\theta) \qquad (8)$$

The direct scattering amplitude is a slowly varying function of energy.

Therefore, when the decomposed amplitude is substituted in Eq. 7, the direct scattering portion can be pulled outside the summation and the Bessel function additional rule gives

$$f_N(E_i,\theta) = J_N(\bar{\alpha}.\bar{Q})f^D(E_i,\theta) + \sum_k J_{N-k}(\bar{\alpha}.\bar{k}_f)f^R(E_i \pm k\omega,\theta)\ J_k(-\bar{\alpha}.\bar{k}_i)$$

It is obvious if there is no resonance then Eq. 2 is recovered.

Now the important point is that Bessel functions have zeros. If we take the Bessel function for N = 1, which for the laser we used will give the strongest signal, then $J_1(0) = 0$. This condition is fulfilled when $\hat{\epsilon}.\bar{Q} = 0$ i.e. when the laser polarization is perpendicular to the momentum transfer direction. Then

$$f_N(E_i,\theta) = \sum_k J_{N-k}(\bar{\alpha}.\bar{k}_f)\ f^R(E_i \pm k\omega,\theta)\ J_k(-\bar{\alpha}.\bar{k}_i) \quad (10)$$

which depends only on the resonant scattering amplitude. The Bessel functions decrease rapidly for increasing N and fixed argument as soon as the value of the order becomes larger than the value of the argument.

Thus we see that with the correct choice of the kinematical vectors of the incident and scattered electrons with respect to the laser polarization it is possible to completely suppress the direct scattering amplitude. This leaves only the resonant part of the scattering amplitude and one should be able to experimentally observe the plure Breit-Wiegner profile. It was the purpose of this work to try and observe this predicted effect.

3. Experimental Considerations

In this section we will discuss the considerations and some aspects of the experimental approach we have used. Firstly, we will show how the use of a laser with its subsequent mode structure alters slightly the soft photon

approximation. Then, we will see under what conditions the best signal can be achieved. Finally, we will give a brief description of previously published free-free experiments, pointing out where our experiment is different.

3.1 Free-free transitions in a realistic laser field

The approximations used to calculate the free-free scattering cross section in the previous section all depended on a description of the laser field as a homogeneous, linearly polarized, plane wave. Of course the lasers with which one would carry out an experiment are not plane waves. Even if the laser operates in single mode, the light beam will have a spatial intensity dependence. In most cases, in order to obtain high light beam intensities, the model purity must be sacrificed giving rise to a very complicated mode structure. Similarly the laser may well be pulsed in which case in addition to the spatial intensity variation there is also a compilated temporal variation present. This requires a slight modification to the soft-photon approximation as described by Jung.[5] The free-free cross section within this approximation for an N-photon transition is redefined as

$$\frac{d\sigma_{ff}(N)}{d\Omega} = \frac{k_f}{k_i} \cdot R_N \cdot \frac{d\sigma}{d\Omega} \qquad (11)$$

where

$$R_N = \frac{1}{T} \int_T \int_V w(\bar{x})\ J_N^2\ [\bar{\alpha}(\bar{x}.t]\ dx^3 dt$$

$w(\bar{x})$ is the density of electron-atom collisions at the point $\bar{x}$, T is the laser pulse length and x and t refer to the spatial and time variables. The free-free cross section has been integrated over the spatial and temporal variation of the laser field. The previously obtained sum rule, Eq. 4, then

becomes

$$\sum_{N=-\infty}^{+\infty} R_N = 1 \qquad (12)$$

This equation can then be tested experimentally by measuring the ratio of the free-free to the elastic scattering peak.

3.2 Relative free-free cross sections - choice of experimental geometries

In order to observe free-free transitions, the laser field has to be applied to the scattering region and scattered electrons near the region of the elastic peak must be measured. The electrons which have undergone a free-free transition show up as satellite peaks spaced by an integral number of photon energies on either side of the elastic peak. In Section 2.1 the advantage of using a laser of low frequency in order to gain signal was shown. For the laser power available to us, we can expect significant probability only for the $N = \pm 1$ free-free transition which is the side peak closest to the elastic peak. Since the electron spectrometer has a finite energy resolution it is difficult to observe a weak free-free signal close to a very strong elastic peak even when the experimental conditions are optimized for maximum free-free signal. Consider for example, the case of a CO_2 laser with $\hbar\omega$ or 117 meV. Typical spectrometer resolutions are 40 meV and with $\Gamma^2 \sim 10^{-4}$ then for every 10^4 elastically scattered electron only one will be detected from a free-free transition. In addition, we have to consider that for our resonance studies, we have to select an experimental arrangement which eliminates direct scattering. Thus only the resonance process will contribute to the signal. Resonance studies on rare gases indicate that the elastic resonance cross sections are of the order of 5 to 40% of direct elastic scattering cross

sections. It is reasonable to assume that the resonances in the free-free cross section will be of the same order of magnitude. Thus one can see it is important to choose conditions very carefully to satisfy all conditions required for the measurements and to be able to generate observable signals.

From Eq. 6 we can see that the free-free cross section can be written as

$$\frac{d\sigma_{ff}}{d\Omega} = K \cdot E_i \cdot \sin^2 \frac{\theta}{2} \cdot \frac{d\sigma}{d\Omega} \qquad (13)$$

The constant K contains all the laser parameters i.e. the power density and the laser polarization. We can now use this equation to evaluate relative free-free cross sections as a function of energy and scattering angle for a number of potential targets. We will consider only rare gases since beams of their atoms are easily produced, the inelastic scattering channels are far removed from the elastic channel and they have well characterized resonances.

Firstly, in Fig. 3.1 we show the differential elastic scattering cross sections for He, Ar, and Xe at incident energies near their resonances.[6,7,8] It can be seen that both Xe and Ar have larger cross sections than He at all angles in the case of Xe and all but a few angles in the case of Ar. He has the strongest resonance in its elastic channel. Secondly, in Fig. 3.2 we have evaluated $d\sigma_{ff}/d\Omega$ as a function of scattering angle at the same energies as indicated in Fig. 3.1. At small and intermediate scattering angles Xe has the largest cross section while at angles beyond 130° it is Ar which has the largest cross section.

3.3 Previous experimental work

The first crossed beam experiments on free-free transitions were carried out by Andrick and Langhans.[9] In their experiment a CO_2 laser of 50 watts power was used in a c.w. mode. This gave a power density of 2×10^3 W cm^2 when

focussed down to the size of the electron beam. The scattering geometry chosen was that of large momentum transfer. At a scattering angle of 160° and an incident energy of 10 eV this gives a value of $\Gamma^2 \sim 10^{-4}$. They were able to observe the N = 1 photon transitions on either side of the elastic peak for scattering from Argon. Figure 3.3 shows an energy loss spectrum they obtained by them. The free-free peaks are immediately obvious. They used specially shaped electrodes in the electron energy analyzer to reduce the spread of the wings of the elastic peak so that the free-free peaks stand out more. In order to test the soft photon approximation of Eq. 5 they measured the ratio Γ^2/F at a number of incident electron energies from 5 eV to 16 eV. Their ressults are shown in Fig. 3.4 and show fairly good agreement with theory. There is some disagreement at 5 eV ($\hbar\omega/E \sim .023$) possibly indicating a break down of the soft photon approximation.

Work on multiphoton free-free transitions (N > 1) has been carried out by Weingartshofer and coworkers.[10-,11] In order to obtain high power densities of 10^6-10^8 W cm^{-2}, they used a pulsed CO_2 laser with a multimode structure. They have measured free-free spectra from both Ar and H_2 for a number of incident energies and scattering angles and also for two laser polarization directions with respect to the scattering plane. Their values of Γ^2 would have been typically about 50. Because of this, the higher order Bessel functions have values which began to become comparable with the lower order functions and so transitions of order N ~ 10 were observed. As their laser was pulsed and had a multimode spatial intensity distribution they tested the sum rule Eq. 12 for a number of values of the of scalar product $\hat{\epsilon}(\bar{k} - \bar{k}_f)/2k_i$. This was done for different time segments of their laser pulse which then represented quite different values of power density.

In Fig. 3.5 we show the temporal variation of their laser pulse. For

instance, the power density corresponding to segment A is 7×10^8 W cm^{-2}. The value for segment B would be down by about a factor of 3 and that for segment C again down by a further factor of 5 or 6. As examples of their results we show Fig. 3.6 which is for the two polarization directions. It is very interesting to observe that in the case where the laser polarization is perpendicular to the scattering plane (and hence perpendicular to $\bar{k}$, $\bar{k}_f$ and $\bar{k}_i - \bar{k}_f$, so that the free-free cross section is zero in the soft photon approximation) some free-free signal is observed. No explanation is given for this but considering that they generally get very good agreement with the soft photon approximation sum rule it is likely that their laser is not 100% polarized in a particular direction.

The only experiment so far which has looked at resonances in the free-free cross section has been carried out by Langhans.[12] Using the apparatus of Andrick and Langhans,[9] he measured the N = -1 free-free cross section in the region of the core split resonances ($^2P_{1/2}$, $^2P_{3/2}$) of Argon at 11.270 and 11.098 eV, respectively. His results are shown in Fig. 3.7. As described in Section 3.2, for each resonance in the elastic channel two resonances separated by $\hbar\omega$ are observed in the N = -1 free-free channel. Langhans also calculated the cross section in soft photon approximation using measured elastic scattering phase shifts. This is shown in the figure as the full line and, clearly there is good agreement between theory and experiment. It is interesting that the observed shape of the resonance in the free-free channel is very close to that in the elastic channel. Langhans had no control over his laser polarization direction and so was not able to observe the resonances for different values of the scalar product $\hat{\varepsilon}.(\bar{k} - \bar{k}_f)$ and hence possibly observe the suppression of the direct scattering background leaving the pure resonant contribution. It is also important to note that a spectrum such as that shown in Fig. 3.7 took up

to 100 hours to accumulate - a very long time in terms of the period of stability the operating conditions of both the laser and electron impact spectrometer.

3.4 Outline of the experimental approach

The aim of our experiment was to observe resonances in a free-free channel under conditions where the direct scattering contribution to the observed cross section is predicted to be suppressed leaving only the resonant portion. In order to do this it was first necessary to observe free-free transitions in the direct scattering channel under optimal conditions before going on to look at resonant scattering.

An energy resolution of between 30-50 meV is required for the electron impact spectrometer since the laser photon energy is 117 meV. More importantly, the line profile for elastic scattering should be as narrow as possible and without wings. The laser output power was 1200 watts but only about half of this could actually be delivered into the vacuum system. The experiments carried out to initially observe free-free transitions used Argon as a target gas at an incident energy of 10.6 eV and at a scattering angle of 141° (which was the maximum possible with our apparatus). The laser was in the scattering plane and the angle between the laser polarization and the momentum transfer vector was 12°. Using a laser spot size of approximately 1 mm in diameter and hence a power density of 7.6×10^4 W cm^2, we obtain $\Gamma^2 \sim 4 \times 10^{-3}$.

For the experiments in resonance scattering it was necessary to choose a scattering angle of 90°. This was achieved by introducing the laser beam perpendicular to the scattering plane. This arrangement gave full control over the scalar product between the laser polarization and the momentum transfer vectors. Under these conditions the optimum target gas was Xe as shown by the relative free-free cross sectins in Fig. 3.2. In this experiment the maximum

value of Γ^2 was ~ 2 x 10^{-3} when the laser polarization was parallel to the momentum transfer vector. (The ratio between the free-free peak and the elastic peak has been reduced by a factor of two as compared to the Argon experiment described above.)

It is interesting to see how our experimental conditions relate to those of previous investigators. In Fig. 3.8 we have plotted $J^2(x)$ vs x for N = 0,1 and indicated on it the values of x for the various experimental groups.

4. The Experimental Apparatus

4.1 The vacuum system

The experiments were carried out in a cylindrical non-magnetic stainless steel vacuum chamber. Its diameter was 24" and its height 20". Just inside the walls of the chamber was an enclosed cylinder of annealed mu-metal shield to prevent penetration of the earths magnetic field. Various ports and flanges allowed attachment of the pumping components and also the electrical connections to the outside. One co-linear set of flanges, offset from the center, were used to mount windows for the laser beam to enter and exit the chamber.

Pumping of the system was done with an 8" oil diffusion pump backed by a mechanical rotary pump. Between the diffusion pump and the chamber was a liquid nitrogen trap to prevent backstreaming of oil vapor from the pump. A second smaller (2") diffusion pump was also added to allow for the possibility of differentially pumping the electron gun. Pressure was monitored with thermocouple and ionization gauges. The base pressure in the chamber was about 1 x 10^{-7} torr and typical operating pressure when the gas jet on was a few times 10^{-6} Torr. A pressure trip ensured that in the event of a sudden increase in pressure whether due to operator error or a system failure then sensitive electronics were switched off and the chamber isolated from the diffusion pump.

4.2 The electron spectrometer

There were two important characteristics required from the electron spectrometer to be used in these studies. Firstly, because the energy of the CO_2 laser photon is 117 meV, it was desired that an instrumental energy resolution of 30-50 meV with a reasonable incident beam current (~10^{-9} Amps.) be achievable. Secondly, because of the very low signal levels expected, it was important that the contribution of the wings of the elastic peak to the general background signal in the free-free transition regions be minimized.

Initially, performance tests were carried out on a spectrometer utilizing single sets of hemispherical energy dispersing elements in both the monochromator and anlayzer. With this device it was not possible to achieve the required conditions. It was then decided to manufacture a new spectrometer which was identical, to one already used at JPL and whose characteristics were suitable and well known. The new spectrometer was made of titanium The difference between this instrument and the one tried previously was (besides the material) that instead of a single set of hemispherical energy dispersing elements in the monochromator and analyzer there were two in tandem. This double dispersion did not only increase resolution but also greatly improved the profile and wing conditions compared to that from a single set of hemispheres. Schematic diagrams of both monochromator (gun) and analyzer (detector) are shown in Figures 4.1 and 4.2.

The operation of the spectrometer is as follows. Electrons are emitted from a heated filament wihtin the cathode housing of the monochromator. This cathode is at a negative potential equal to the desired beam energy with respect to ground. A series of electrostatic lenses focuses the electrons at the entrance to the double hemispheres. This virtual image is dispersed in energy and refocussed at the exit to give an image linear in energy at the exit side.

Only a section of this energy dispersed image is selected by a lens system which contains the actual window and pupil. The energy selected beam then focused onto the target atomic beam. Hence, starting with a Maxwellian energy distribution of about 0.5 eV full width half maximum at the filament, a beam is produced with a width of about 25 meV.

The analyzer works in a very similar manner to the monochromator. Electrons which enter the analyzer within the viewcone defined by the nose cone and the aperture A_2 (Fig. 4.2) are focussed by an achromatic lens train at the entrance to the double hemispheres. After double dispersion and energy selection they are then refocussed at a channel electron multiplier where they are detected.

The overall resolution of the instrument is a convolution of the individual resolutions of the monochromator and analyzer. At an incident current of greater than 1 nA a resolution of 40 meV couldbe readily achieved. The line profile was very good but it was better on the superelastic side than on the inelastic side of the elastic peak. The angular resolution of the analyzer entrance was about 5°.

Circuitry and voltage divider networks for the control of the electron optics were designed and built but details will not be given here. There are a number of modes in which the spectrometer can be operated and we will describe the two of relevance to this work.

Firstly, in the energy loss mode we measure the energy spectrum of the scattered electrons. The incident energy and scattering angle are fixed while electrons are counted as a function of the energy loss (or equivalently residual energy) of the scattered electrons in collision with a target gas atom. Without the laser field, the possible values of energy loss range from zero (elastic collision) to the value of the incident energy. If the incident energy

is below the first excitation threshold then only elastically scattered electrons can be observed. With the laser on, as described earlier, it is possible for the scattered electrons to have gained or lost integral units of the photon energy. By measuring the electron energy spectrum around the elastic region, it is possible to observe whether any electrons have made a free-free transition through interaction with the laser field.

Secondly, it is possible to select a particular value of energy loss or gain and then measure the signal in this channel as a function of the incident electron beam energy at a fixed scattering angle. This way resonances in the particular cross section can be identified.

The target gas beam for the spectrometer was formed by flowing the gas through a micro-capillary array which was inserted into a 1 mm diameter tube. This gave a well collimated dense beam of atoms.

4.3 The laser and associated optics

In order to observe even the lowest order free-free transition with the present capabilities the laser power density must be of the order $\sim 10^4$ W cm^2. Power densities of $\sim 10^7$ W cm^2 can be obtained with pulsed CO_2 laser systems but when such a laser is used the free-free cross section is averaged over the spatial and temporal distribution of the light pulse. By use of a c.w. laser with single mode operation this can be overcome. In addition the duty cycle of the pulsed laser is several orders of magnitude lower than for c.w. laser. For our experiments, therefore, a c.w. CO_2 laser was selected.

The laser used was a Photon Sources 1003 Model CO_2 laser installed at the Center for Laser Studies at the Univeristy of Southern California. The laser had an eighteen meter cavity. Its output could be either c.w. or chopped c.w. and the maximum output power was 1200 Watts. Nominally the output mode structure was TEM01 but both mode burns in plexiglass and beam profile

measurements using a scanning slit showed the output to be multimode in nature. The laser had been tuned for maximum power output at the cost of single mode operation. Figure 4.3 shows a beam profile measurement clearly demonstrating the multimode structure.

In Section 2.2 it was shown that we wanted to measure the free-free signal as a function of laser polarization direction with respect to various kinematical vectors. It was necessary, therefore, to determine the laser polarization. According to the manufacturers specifications the output is randomly polarized. This was extensively investigated. The laser output was set a fairly high power level and then the intensity was reduced by a series of apertures and a chopper. A wire-grid polarizer was inserted into the beam and the transmitted power was monitored as the polarizer was rotated. Consistently the laser was measured to be highly polarized. At our work station, just before the beam entered the chamber, the orientation of the polarization was in an anticlockwise direction of 20° to the horizontal when looking along the propagation direction. The transverse polarization was found to be 75-80%. This polarization was attributed to polarizing reflections from a cross-over tube between two sections of the laser cavity.

Figure 4.4 shows a schematic diagram of the laser and its relationship to the vacuum chamber. The beam leaves the laser and is transported along inside aluminum tubes. Water cooled copper turning mirrors allow manipulation of the beam direction to the various work stations on the beam line. After the final turning mirror the laser is focussed down into the interaction region using a 24" focal length lens made from ZnSe which is also water cooled. The beam enters and exits the chamber through NaCl windows which are kept at a few degrees above room temperature to prevent formation of condensation. A power meter collected the beam after it left the vacuum chamber.

For studies involving the linear polarization dependence of the free-free signal, a polarization rotator was purchased from Laser Power Optics and placed in the beam, before the second mirror, in an angle calibrated mount. The transversly polarized laser beam entered the rotator where it underwent a series of reflections and suffered a total phase change of 180° before leaving the device. The output was a transversly polarized light beam but by rotation the polarizer by an angle α, the output beam polarization rotated by an angle of 2α. With this arrangment we had complete control over the laser polarization direction.

When the beam exits the laser its diameter is less than 1 inch but by the time it reaches the lens its diameter has grown greater than 1 inch which is the diameter of the lens. We can estimate the focussed spot diameter which is given by

$$d_o = \frac{4\lambda f}{\pi d} \tag{13}$$

where for a CO_2 laser $\lambda = 10.6$ μm, the lens focal length, $f = 24"$ and the incident beam diameter, $d = 1"$. This gives $d_o \sim .32$ mm. Equation 13 strictly only applies to diffraction limited Gaussian beam optics and thus the calculated beam diameter can only be looked upon at as a lower limit. Mode burns and burns on thermal paper at focus indicated that the actual spot diameter was approximately 1 mm.

We can calculate the depth of focus for the lens at an incident beam diameter of 1". This is given by

$$\delta = \pm 2\lambda(F/\#)^2 \tag{14}$$

where F/# is the f-number of the lens. In our case we get $\delta \sim \pm 1.22$ cm. Thus

the beam remains reasonably tightly focussed over the range of 2.44 cm or approximately 1".

As the laser wavelength corresponds to the infra-red region of the spectrum, it is necessary to have some sort of method to track the laser beam path. This was done by use of a He-Ne laser. When the alignment was being carried out a movable mirror (M_1), controlled by a pneumatic valve switched the He-Ne beam into the path of the main laser beam. Various interlocks insured that the main laser was disabled when this was carried out.

4.4 Data acquisition and analysis

When a scattered electron is detected the pulse from the channel electron multiplier is first amplified by a fast amplifier and then it is fed into a discriminator to reject any noise pulses. At this point the detected signal can be routed to a number of different destinations. Firstly, it can be put into a ratemeter which has the primary use of tuning the electron optics to provide the optimum signal at the best resolution. Secondly, it can be counted on a counter timer. This allows the signal to be counted for a preset time. Finally, the signal can be used as input to a multi-channel scaler - in this case a Norland 5300. This is used in conjunction with both scanning modes of the electron spectrometer. Thus we get a display of the signal as a function of the energy loss or incident energy.

Connected to the multichannel analyzer via an RS232 serial interface was a tape recorder. The data could then be read to a file on the tape. In the early stages of the experiment the tape had to be taken to the Jet Propulsion Laboratory where it was inspected and evaluated on a computer. Later a Tektronix 4052 computer was purchased so that the data could be manipulated directly after collection.

4.5 The experimental geometries

Two experimental geometries were used. These are shown in Figure 4.5. the first geometry was used to observe free-free transitions under optimal signal conditions. It is similar to that used by other groups. The scattering angle was fixed at 141°. The gas beam originated from beneath the scattering plane in and was perpendicular to it. The laser beam was in the scattering plane and the polarization of the laser was at an angle of 20° with respect to the scattering plane. The projection of the laser polarization in the scattering plane was at an angle of 12° to the momentum transfer vector $\bar{Q}$.

In the second case which was used to attempt to observe resonances in the free-free channel the laser was perpendicular to the scattering plane. The scattering angle was fixed at 90° but the laser polarization could be set at any angle in the scattering plane. The gas beam was slightly out of the scattering plane so as not to direct the bulk of the gas flow into the entrance of the energy analyzer.

5. Results

5.1 Direct scattering

Free-free transitions can only arise when there is an overlap of the electron, atom and laser beams. If there is not complete overlap between the beams then the measured signal is reduced e.g. only a part of the laser beam may be irradiating the interaction volume of the electron and the atom beam and the rest is wasted. It is easy to imagine such a situation arising since all the beams are of the order of 1 mm in diameter. Hence, it is important, because of the small signal levels involved, that there is a maximum amount of overlap.

Initially the CO_2 laser is aligned with the He-Ne beam and this is made to cross the scattering center defined by the crossing of the atomic and electron beam axis. This was all achieved by optical alignment. The true scattering

center defined by the crossing of the electron beam and atom beam maximum flux densities, however, may be slightly off from the optically defined geometrical scattering center. The following method was used to insure that he best overlap condition was found. When the electron spectrometer was tuned, the He-Ne laser was switched on. It was then maneuvered, by means of the verniers in the second turning mirror, so that the focussed spot appeared at the end of the capillary array. Again using the verniers it was moved off the array by a couple of millimeters in the direction of the electron beam. In the case of geometry a) in Figure 4.5 this was done using the vertical vernier control and for geometry b) by use of the horizontal vernier control. At this stage electrons with residual energy of E_o + 117 meV were detected and counted by a scalar. The CO_2 laser was then turned on and the number of electrons was counted as the laser was scanned by the vernier through the electron beam. The electron counts were also measured when the CO_2 laser was off. The maximum in the one photon free-free transition thus defined the optimum overlap condition. The superelastic free-free peak (absorption of one photon) was chosen because the instrumental line profile was slightly assymmetrio - the superelastic side having fewer background counts at 117 meV away from the elastic peak than the inelastic side.

In Figure 5.1 we show the N = +1 free-free signal as the CO_2 laser was scanned through the electron beam using argon target, 12 eV incident electron energy and geometry as indicated in Fig. 4.5a. The smallest vernier division (.001) is equivalent to a translation of the beam of .3 mm in the focal plane and this is small enough that the electron beam can not be skipped over. It is apparent from the diagram that at some vernier readings there are more counts with laser on than with laser off. This represents the detection of electrons which have undergone a free-free transition. At the peak the count rate is only

a few per minute above the background. This is to be expected from our value of Γ^2 in this geometry. In fact if we consider that we were detecting about 100 e^-/s in the elastic peak one might have expected slightly more counts indicating that the overlap between the electron and atom beams may not have been optimum. This may occur if the laser beam at focus had a larger diameter than the electron beam and so all the incident power would not fall on the electron beam. But the fact remains, we were indeed able to observe free-free transitions.

Having found our optimum overlap condition we scanned through the energy spectrum of the detected electrons in the vicinity of the elastic peak to find the satellite peaks spaced at one photon energy on either side of the elastic peak. Such a scan is shown in Figure 5.2 On the energy gain side of the peak one can see at +117 meV an indication of a peak. It is not so apparent on the inelastic side due to the higher level of background counts. It is extremely time consuming to generate this type of spectra because of the large number of channels to be scanned and the large number of scans required to establish acceptable signal to noise conditions in the free-free peaks. From the ratio of the peak heights in Fig. 5.2 we can obtain a power density of 2.9×10^4 W cm^{-2} using Eq. 6. We know from beam burns at focus that the diameter of the laser beam was between 1 and 2 mm.From the beam overlap scans such as Fig. 5.1 we see that only one or two vernier positions show counts above the background indicating that the electron beam diameter is less than 1 mm. Hence some of the incident power was wasted. To correct the situation would have required placing a shorter focal length lens inside the vacuum chamber. With the problems of cooling and manipulation, it was felt that because the free-free signal could be detected we would go on using the existing set up.

In Fig. 5.3 we show the free-free signal in the $N = \pm 1$ channel as a function of laser position when the target gas was Xenon, the incident energy

was 7.0 eV and the configuration was that of Figure 4.5b. Measurements were carried out with two laser polarization directions with respect to the momentum transfer direction. The top figure (5.3a) shows the case of $\hat{\varepsilon}.\bar{Q}$ = cos 22.5° and the lower figure (5.3b) the case of $\hat{\varepsilon}.\bar{Q}$ = cos 0. Since the individual measurements took a long time, it can not be surely stated that the scattering geometry (mainly electron beam and laser beam) were the same for the two measurements. Also even under identical conditions, we would expect only 15% difference in the free-free signal for the two cases and better statistics would be required to allow definite conclusions.

5.2 Resonant scattering

Having observed free-free transitions, it was then possible to move on to the resonance experiments. First it was necessary to observe the resonances in the elastic scattering channel. For this purpose we detected electrons which have lost no energy in the collision with the target atoms as a function of electron incident energy at fixed scattering angles. In Table 1 we give a summary of the properties (position and width) of resonances in the elastic channel for He,[13] Ar,[13] and Xe.[14] Figure 5.4 a,b,c show our ressults on these resonances with the θ = 141° scattering geometry of Fig.4.5a. The helium resonance is by far the one largest effect in the elastic cross section (of the order of 40%) and this is followed by the Ne resonance (25%) and the Ar resonances (9%). The Fano profile of the resonance reflects the interference between the direct and resonant scattering amplitudes. The resonance profiles change with scattering angle and in Figure 5.5 we show the Xe($^2P_{3/2}$) resonance at a scattering angle of 90°. The profile has changed from being essentially a dip in the elastic cross section to being an enhancement and the percentage effect has reduced from 25 to 9%.

There is not sufficient information available to make a rigorous selection

concerning the optimum gas species and optimum scattering angle for the observation of the resonance scattering (with supressed direct scattering). Based on semiempirical reasonings, and geometrical constrains in our apparatus, we have selected Xe43 with $\theta = 90°$ scattering geometry for the purpose of our experiments.

In Fig. 5.6 we show our results for the Xe ($^2P_{3/2}$) resonance in the elastic (upper part) and N = +1 free-free channel (lower part) with the CO_2 laser OFF in both cases. In order to make the time requirement reasonable, we carried out the measurements only at five electron incident energies (E_o = E_R-3/2 $\hbar\omega$; E_R-$\hbar\omega$, E_R-1/2 $\hbar\omega$, E_R and E_R + 1/2 $\hbar\omega$). The resonance clearly shows up in the elastic channel at $E_o = E_R$ and no signal above the general background is observed in the N = +1 free-free channel as expected in the absence of the laser field.

In Fig. 5.7 we show the results obtained with the laser ON and ε $\hat{p}$arallel with $\bar{Q}$. The laser power at the scattering center was about 600 watts focused down to a spot size of about 1-2 mm in diameter. Our previous estimation of the power density incidates that this corresponds to about of 2.9 x 10^4 Watts/cm^2. In this case the laser polarization was set parallel to the momentum transfer vector and the laser was chopped by a chopper placed on front of the polarization rotator. The chopper controlled the channel advance of the multichannel analyzer and alternate channels recorded the laser ON and laser OFF counts. Counts in alternate channels were then summed on the computer at the end of the counting period. By chopping the laser beam, we moderated the heating both for the laser ON and the laser OFF cases of the elements in the laser beam path and maintained an identical steady state temperature. The error bars shown are the square root of the number of counts detected although strictly speaking this is only valid for much larger numbers. From the work of

Langhans[12], one would expect the resonance shape in the free-free channel to be the same as that in the elastic channel. So we would be looking for about a 9% effect in the difference between the laser ON and laser OFF counts at $E_o = E_R - \hbar\omega$ and E_R. As can be seen from the plot there is no clear-cut evidence for the resonance either at the resonance energy or at the resonance energy minus one photon energy. This must be entirely due to the poor statistics.

For completeness we show in Fig. 5.8 measurements in the vicinity of the resonance when the laser polarization was set perpendicular to the momentum transfer direction and thus the direct free-free scattering was eliminated. In this case we see that the laser on and laser off counts are much closer together than in the case where $\hat{\varepsilon}.\bar{Q} = |\omega Q|$ although again the statistics are poor. This does seem to indicate that we have in fact suppressed the non-resonant free-free transitions, although, at the positions E_R-1 and E_R there is little sign of a resonant signal being present. The reasons for this is again poor statistics.

It should be pointed out that the data taken for Figs. 5.7 and 5.8, which are the crux of the experimental effort were taken within the last few days of the available time for this project and clearly a great deal more time would be required to obtain data with desirable signal to noise conditions.

We can make an estimation of the time required to clearly see the resonance effect in the N = +1 free-free channel ($\hat{\varepsilon}.Q \neq 0$) with the instrumentation available to us. Let us require that the free-free resonance signal, I_R^{FF} be five times as large as the statistical spread in the direct free-free signal, I_D^{FF}, and the background, I^B (all in units of counts per second). From our studies of resonances in the elastic channel we estimate the resonance signal to be about a 10% effect on the direct signal and so we want

$$I_R^{FF} = 5\sqrt{I^B + I_D^{FF}}$$

using estimates of $I^B \sim 3\ min^{-1}$ $I_D^{FF} \sim 1\ min^{-1}$ for the $Xe(^2P_{3/2})$ resonance at 7.77 eV then from

$$1\ I_D^{FF}\ T = 5[(I^B + I_D^{FF})T]^{1/2}$$

where T is the accumulation time required to satisfy the above requirement. We obtain a value of T ~ 160 hrs.

We estimate that our accumulation time of the same order of magnitude would be required to observe the free-free resonance signal when the direct scattering is suppressed ($\hat{\epsilon}.Q = 0$). This is not an impossible requirement since many individual runs can be added up. Considering the very stringent requirement on the various components of the experiment (stability of the electron spectrometer, laser, absence of electronic and electromagnetic perturbations, heating effects, continuous attention and monitoring etc.), it is likely that several months would be required to produce and reproduce just a single set of data to clearly demonstrate the presence of pure resonance signals in the free-free scattering channel.

6. Conclusions

We have assembled an apparatus to study electron-atom collisions in a strong radiation field. The basic electron impact spectrometer was borrowed from the Jet Propulsion Laboratory and time on the CO_2 laser was donated by the Center for Laser Studies at USA. These arrangements certainly saved a great deal of expense and time but adaptation to our particular need still required a very extensive effort. We spent a considerable part of the two years to design,

build and debug the electron optics and to reconfigure the electron spectrometer for the desired scattering geometry. The mode structure, polarization character, stability and alignment of the CO_2 laser had to be established. Proper windows had to be installed into the chamber of the spectrometer and the appropriate optics and polarization control had to be realized. We encountered some difficulty with the polarization rotator. The first procurement yielded a device which could not take the heat load and had to be canceled. A second supplier was found and produced the desired polarized. (This alone took about six months time.)

Before we could attack the main aim of our program (the observation of resonances in free-free channels under conditions where the direct scattering is eliminated), we had to carry out a number of experiments to check our approach and to gradually build up to the final experiments. These steps included

a. Detection of free-free transitions under optimum conditions for direct scattering.

b. Detection of resonances in the elastic channel.

c. Observation of the effect of laser polarization on the free-free signal.

We were able to detect one photon free-free transitions for electron atom scattering from argon, at a scattering angle of 141°, and from xenon, at a scattering angle of 90°, using incident energies in the vicinity of the resonances for these species. To our knowledge we are the first to observe to observe such transitions using xenon as a target atom. The resonances were detected and characterized for He, Ar and Xe.

The main thrust of our experimental program was to observe a resonance in the free-free channel for different values of the angle between the laser polarization and the momentum transfer direction. Because of the low count

rates involved (1-2 minute^{-1}), even in the optimum case where the polarization direction and momentum transfer were parallel, we were unable to observe the resonance. We estimate that in order to observe the resonance, counting times of the order of weeks would be required. That time was not available to us. (We were allowed to use the laser only when it was not needed for the research carried out by the Center for Laser Studies and the electron impact spectrometer on loan from JPL had to be returned after the two year loan period.) There was an indication from our studies that the free-free cross section vanished, in accordance with the soft photon approximation, when the laser polarization and momentum transfer were perpendicular. Because of poor statistics, we were unable to test the theoretical prediction of Jung and Taylor.[4] However, we found nothing in our studies to indicate the experiments necessary to check this theory could not be done with the investment of considerably more time and/or higher laser power.

Acknowledgements

We would like to thank Professor Michael Bass and the staff and students of the Center for Laser Studies at USC for all their help throughout the period of this work and for letting us use their CO_2 laser. Considerable help from and valuable discussions with Professor Roy Newell, University College, London, UK is also gratefully acknowledged.

References

1. Kroll N. M. and Watson K. M. 1973 Phys. Rev. A 8 804-809.
2. Mittleman M. H. 1982 Comment. At. Mol. Phys. 11 91-100.
3. Kruger H. and Schulz M 1976 J. Phys. B: At. Mol. Phys. 9 1899-1910.
4. Jung C. and Taylor H. S. 1981 Phys. Rev. A 23 1115-1126.
5. Jung C. 1980 Phys. Rev. A 21 408-411.
6. Register D. F., Trajmar S. and Srivastava S. K. 1980 Phys. Rev. A 21 1134-1151.
7. Srivastava S. K., Tanaka H., Chutjian A. and Trajmar S. 1981 Phys. Rev. A 23 2156-2166.
8. Trajmar S. 1982 private communication.
9. Andrick D. and Langhans L. 1978 J. Phys. B: At. Mol. Phys. 11 2355-2360.
10. Weingartshofer A., Clarke E. M., Holmes J. K. and Jung C 1979 Phys. Rev. A 19 2371-2376.
11. Weingartshofer A., Holmes J. K., Sabbagh J. and Chin S. L. 1983 J. Phys. B: At. Mol. Phys. 16 1805-1817.
12. Langhans L. 1978 J. Phys. B: At. Mol. Phys. 11 2361-2365.
13. Brunt J. H., King G. C. and Read F. HG. 1977 J. Phys. B: Atm. Molec. Phys. 10 1289-1301.
14. Kuyatt C. E., Simpson J. A. and Mielczarek S. R. 1965 Phys. Rev. A 138 385-399.

Table 1

Summary of Resonance Properties

Species	Configuration		Width (meV)	Position (eV)
He	2^2S		9 ± 1	19.366 ± 0.005
Ar	$2p^5\ 3S^2$	$^2P_{3/2}$	2.5 ± 0.5	11.098 ± 0.010
		$^2P_{1/2}$	---	11.270 ± 0.010
Xe	$5p^2\ 6s^2$	$^2P_{3/2}$	4.5 ± 1.0	7.77
		$^2P_{1/2}$	---	9.05

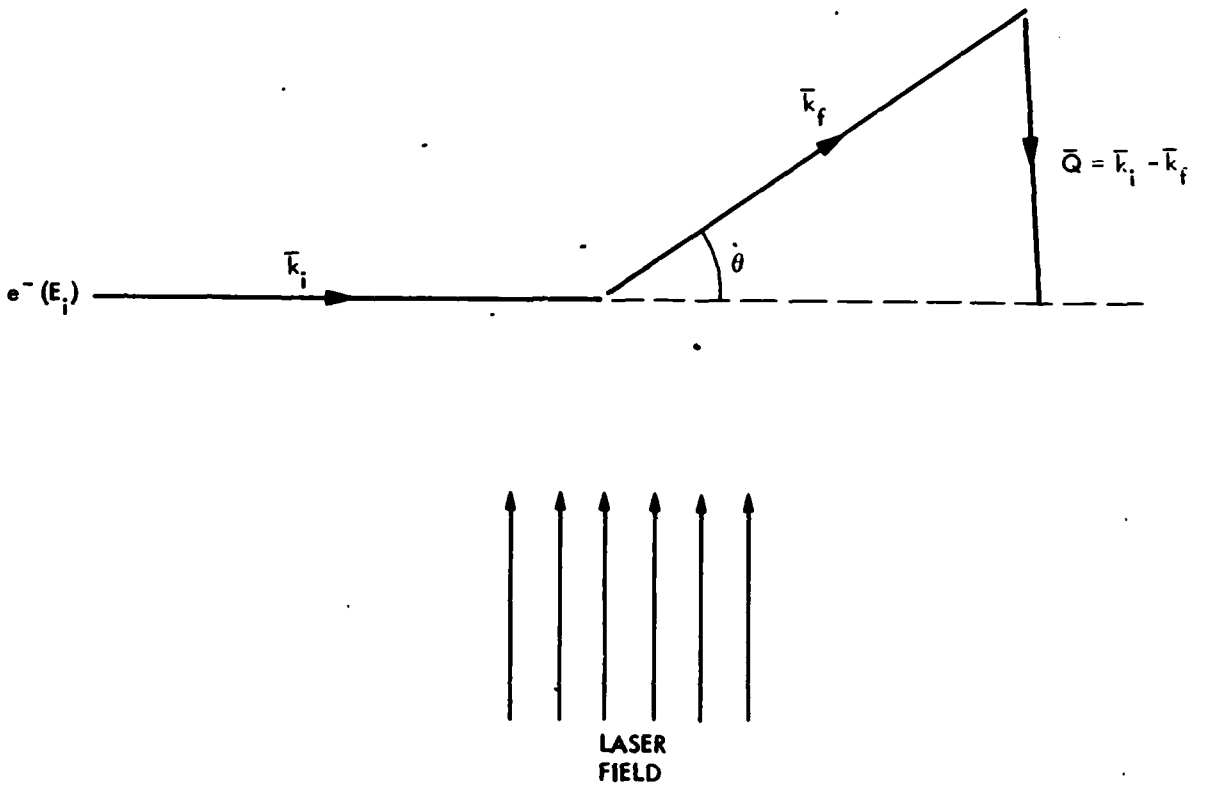

Figure 2.1. The scattering geometry.

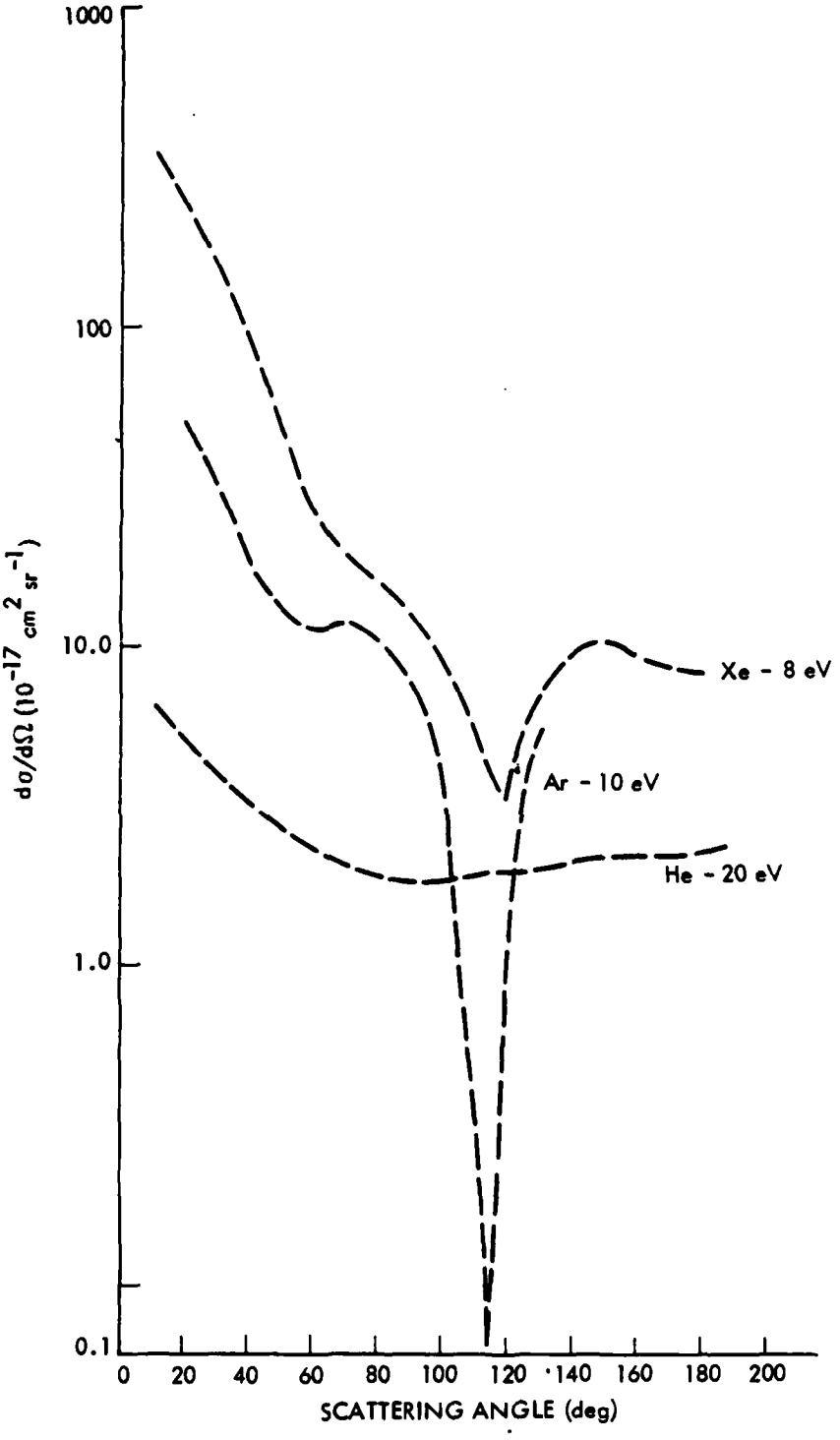

Figure 3.1. Differential cross-sections for Xe, Ar and He near the region of their resonances.

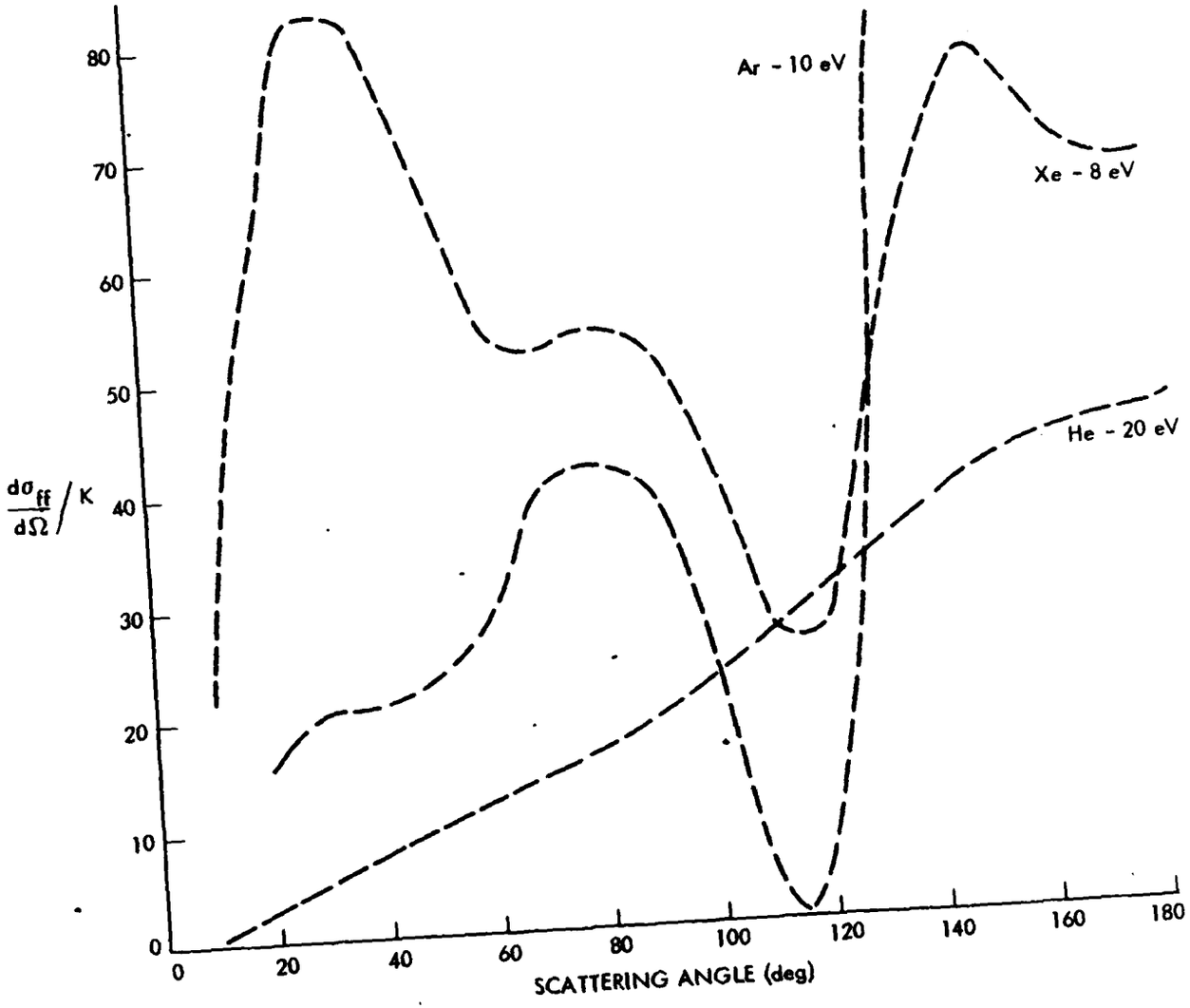

Figure 3.2. Free-free cross-section for direct-scattering near a resonance.

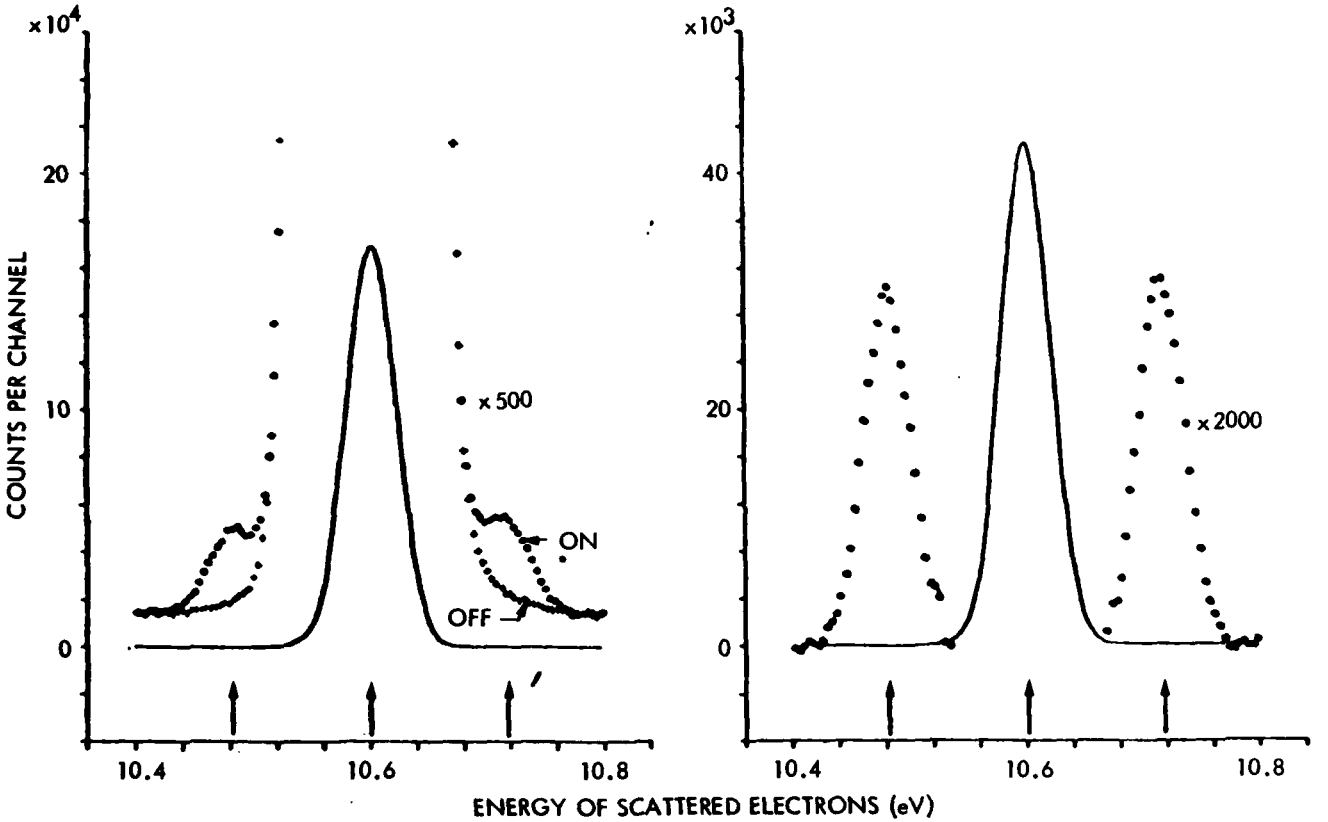

Figure 3.3. Observation of N = ±1 free-free transitions by Andrick and Langhans (E_i = 10.6 eV, $\theta = 160^o$.

The signals with laser ON and OFF are indicated on the left. The difference of the free-free signal and the elastic signal is indicated on the right).

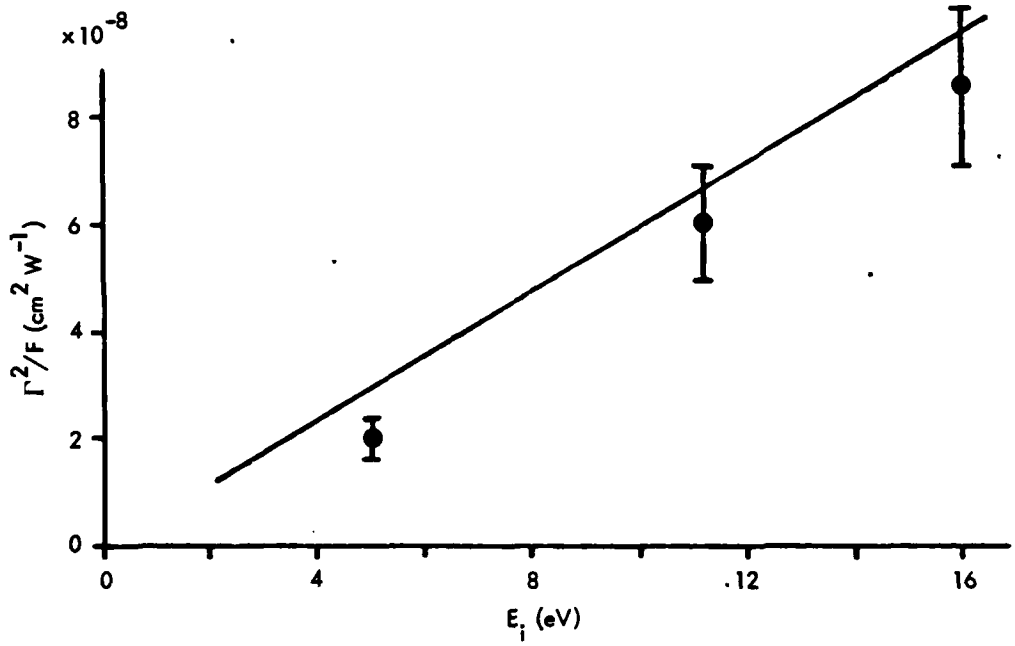

Figure 3.4. Test of the soft photon approximation by Andrick and Langhans. Straight line, soft photon approximation; ⧳, their results.

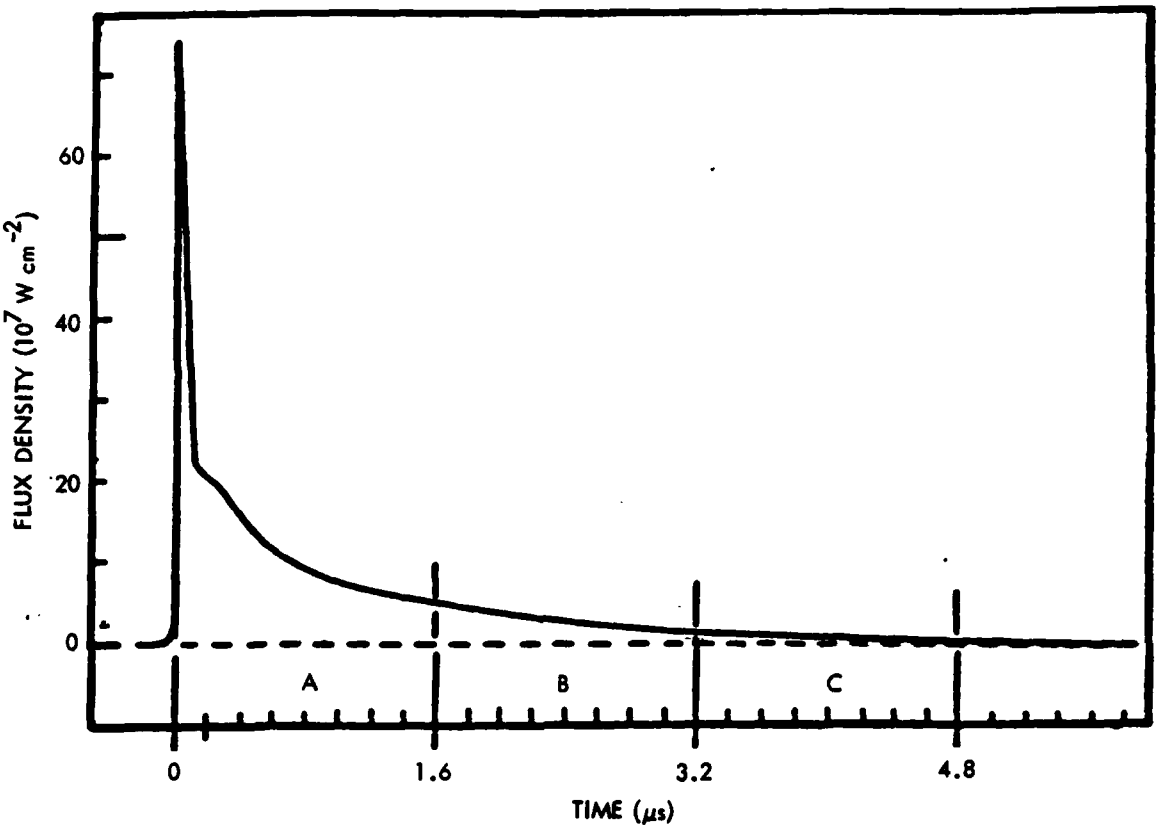

Figure 3.5. Temporal behavior of the laser pulse used by Weingartshofer et al. (The fine structure, subnanosecond oscillations are not indicated.)

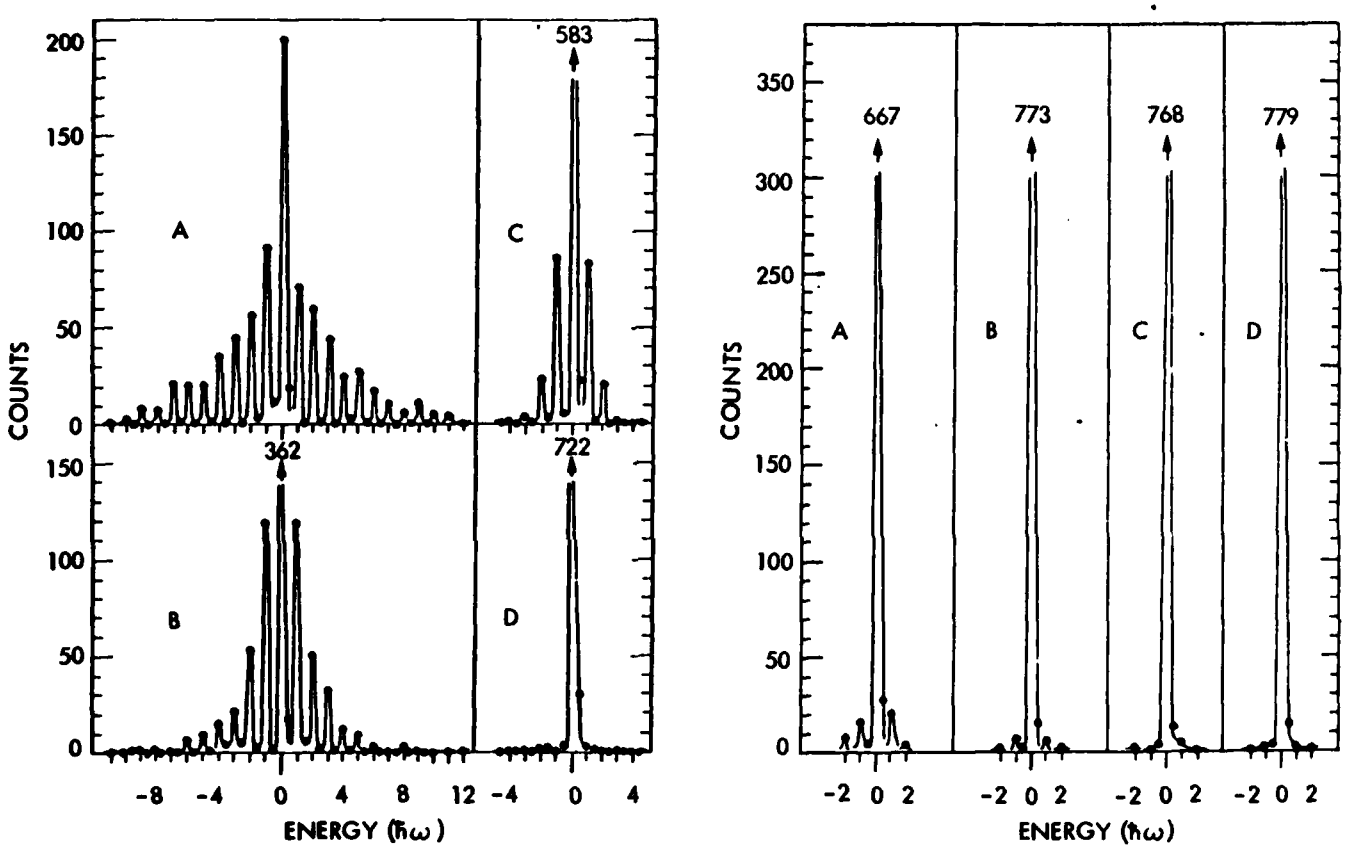

Figure 3.6. Observations of free-free transitions by Weingartshofer et al. Left side: $\hat{\epsilon}$ is parallel to scattering plane, E_i = 9.9 eV; $\theta = 155^o$. Spectra A, B, C and D were obtained at temporal regions indicated in Figure 3.5. The energy of the scattered electron is given in units of laser photons. Right side: $\hat{\epsilon}$ is perpendicular to the scattering plane, E_i = 9.9 eV, $\theta = 8^o$.

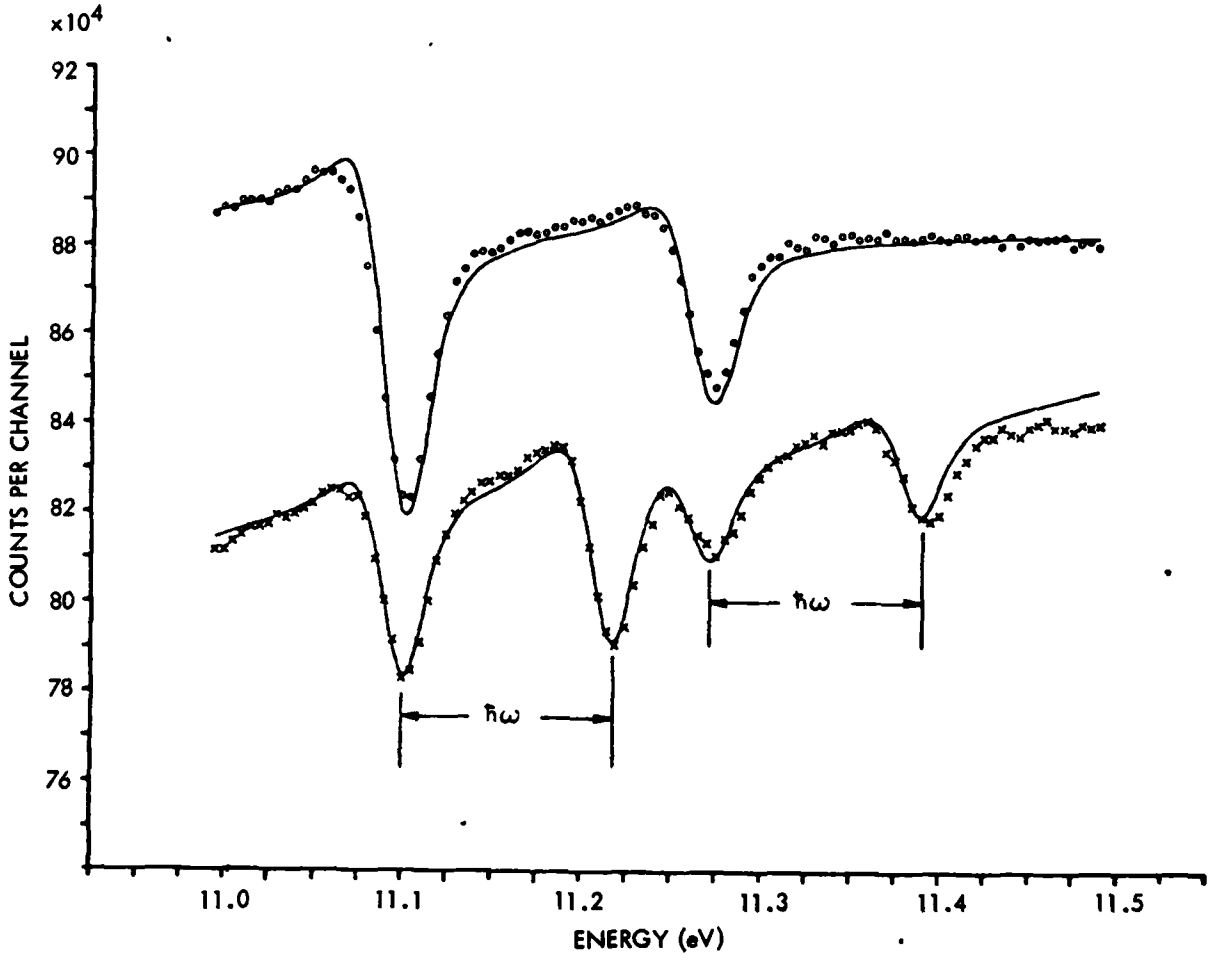

Figure 3.7. Observation of the Ar ($^2P_{3/2}$, $^2P_{1/2}$) resonances at 160° scattering angle by Langhans. Upper curve: elastic channel. Lower curve: N = -1 free-free channel.

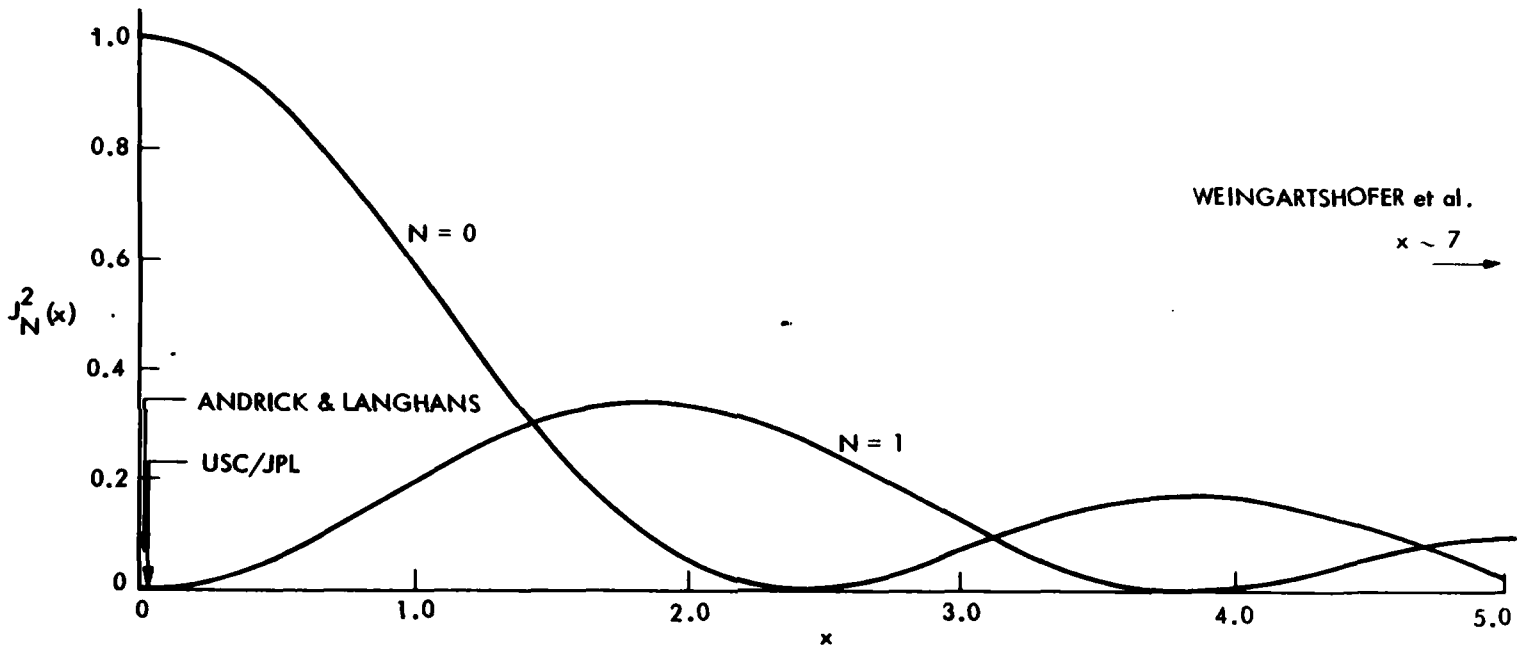

Figure 3.8. Plot of $J_N^2(x)$ for N = 0,1.

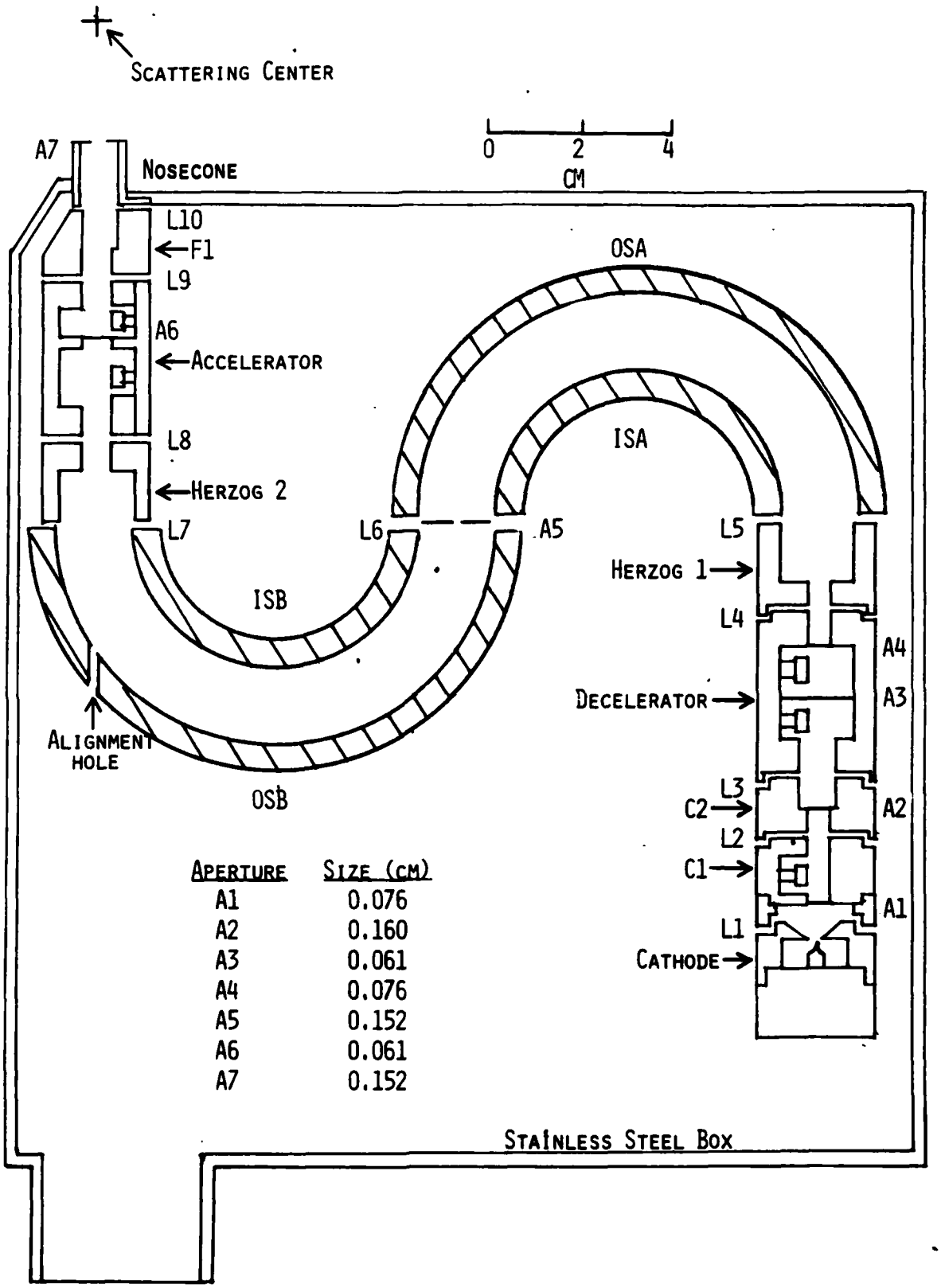

APERTURE	SIZE (CM)
A1	0.076
A2	0.160
A3	0.061
A4	0.076
A5	0.152
A6	0.061
A7	0.152

Figure 4.1. Double hemispherical monochromator.

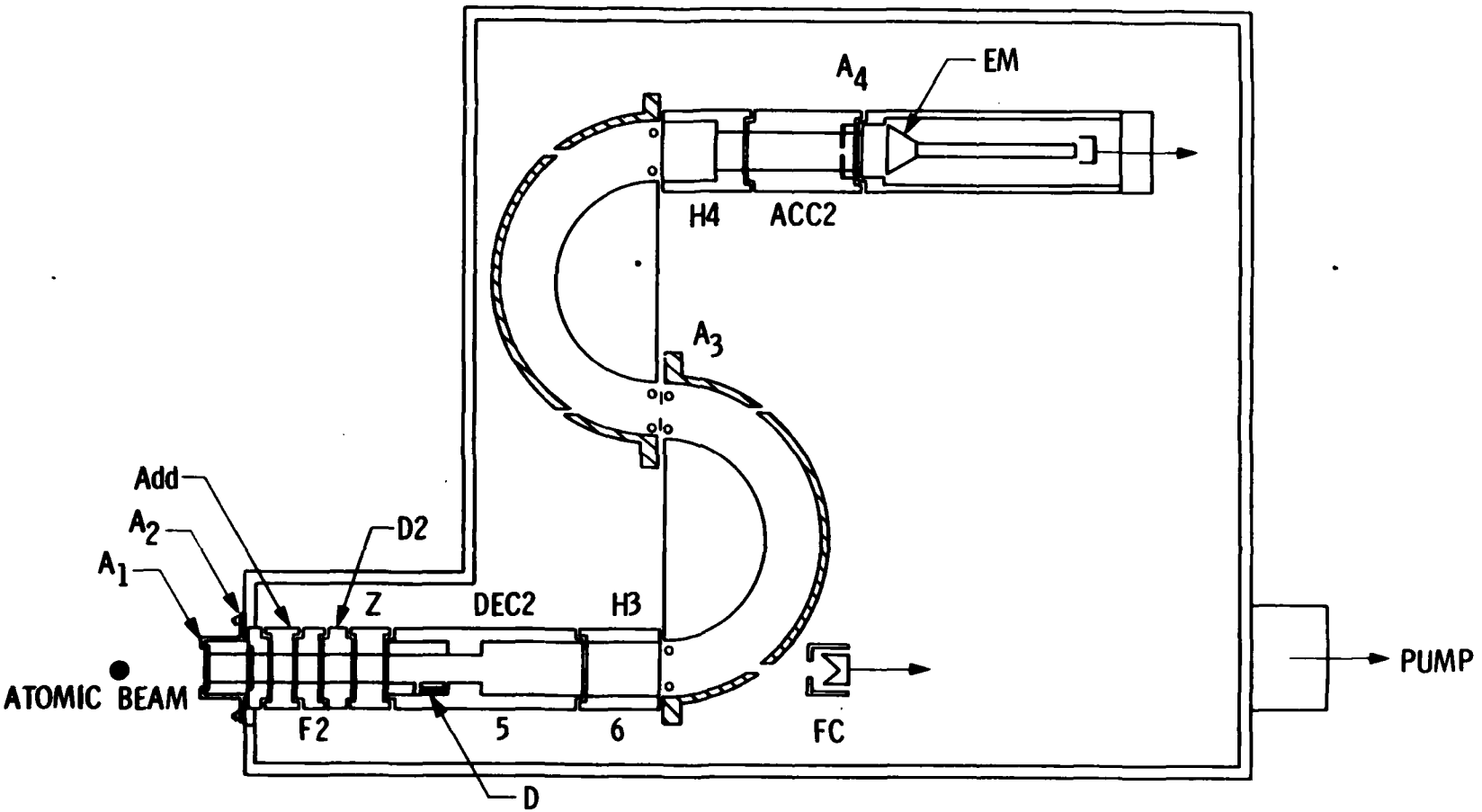

Figure 4.2. Double hemispherical analyser.

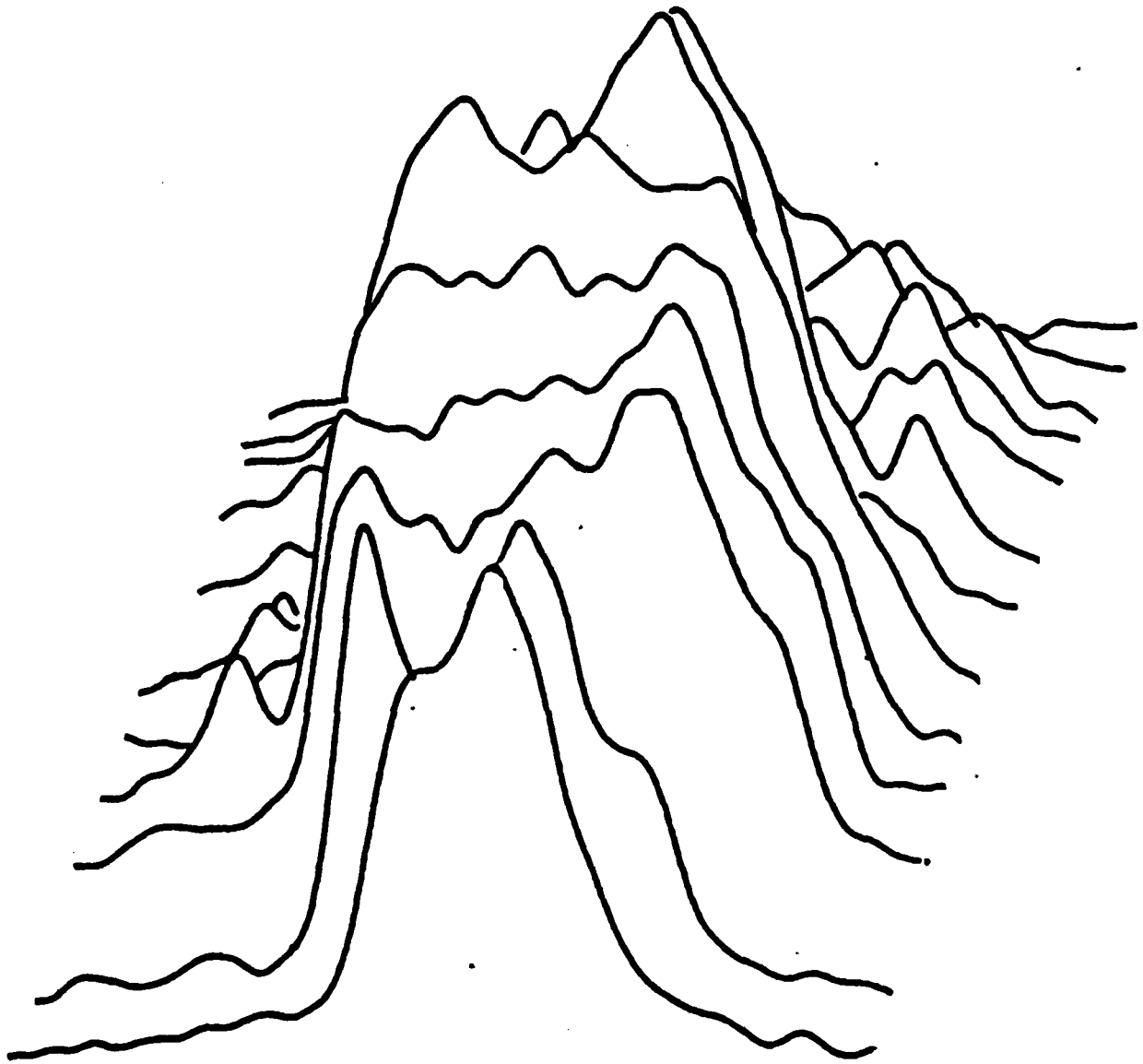

Figure 4.3. The laser beam spatial distribution profile.

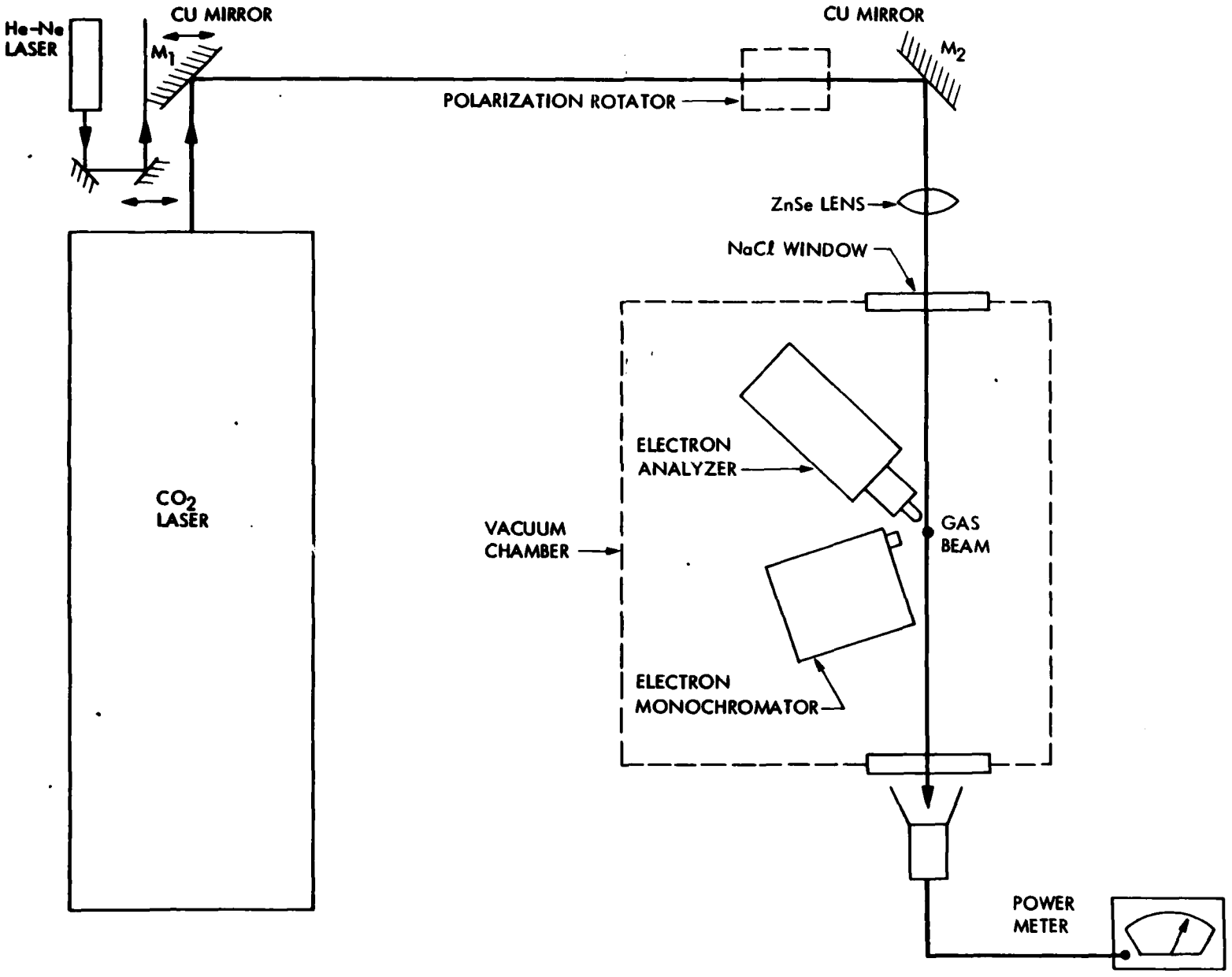

Figure 4.4. The experimental set up

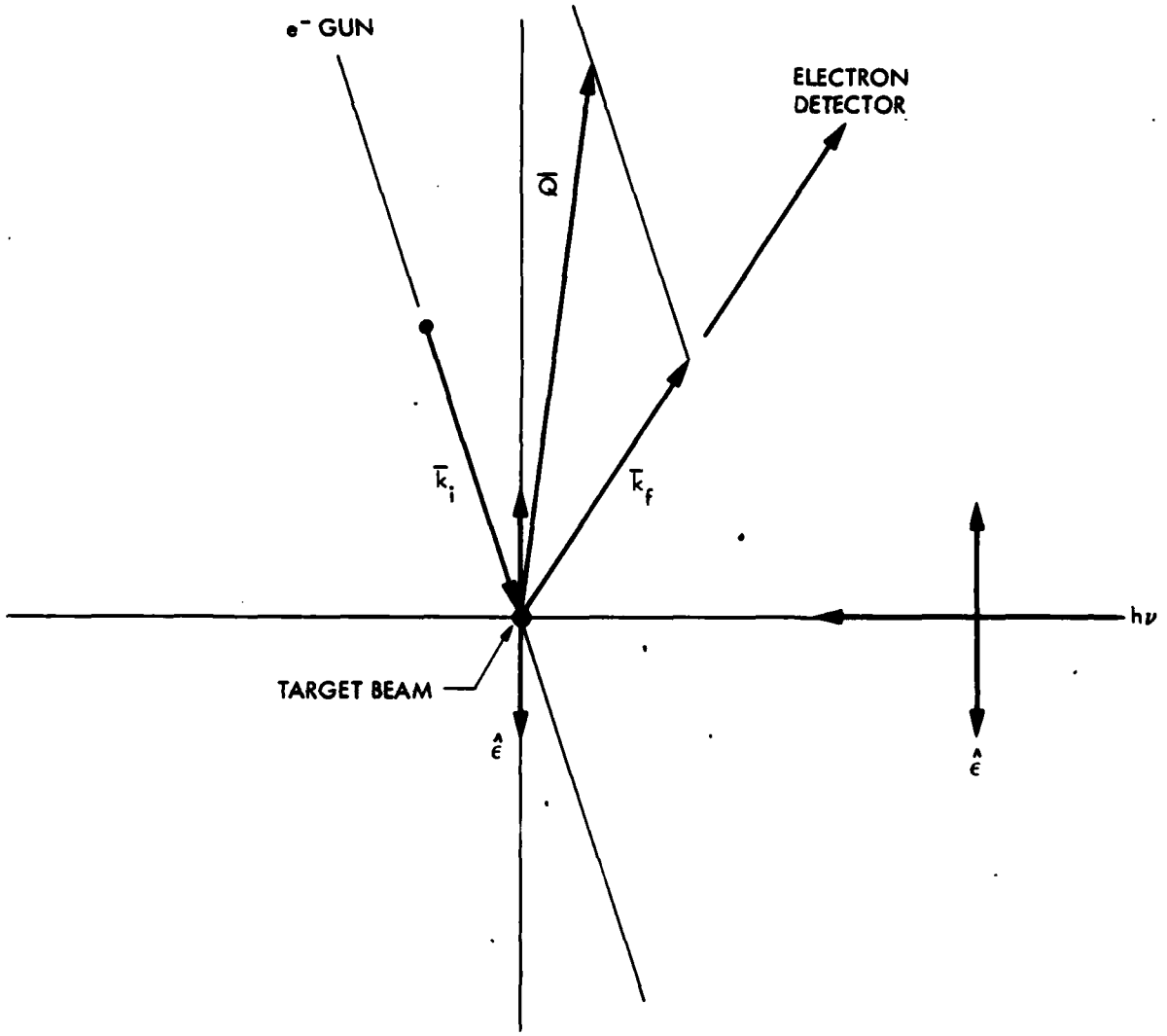

Figure 4.5a. The $\theta = 141^{\circ}$ scattering geometry. Laser beam is in the scattering plane.

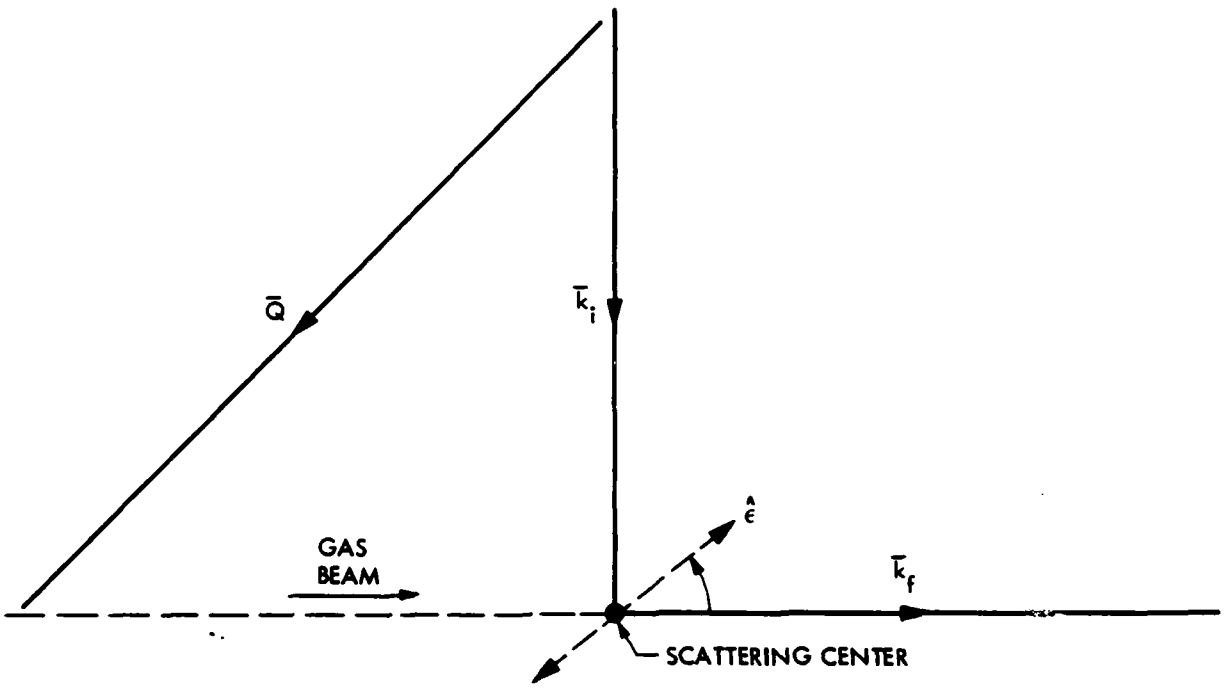

Figure 4.5b. The $\theta = 90^{o}$ scattering geometry. Laser beam is perpendicular to the scattering plane.

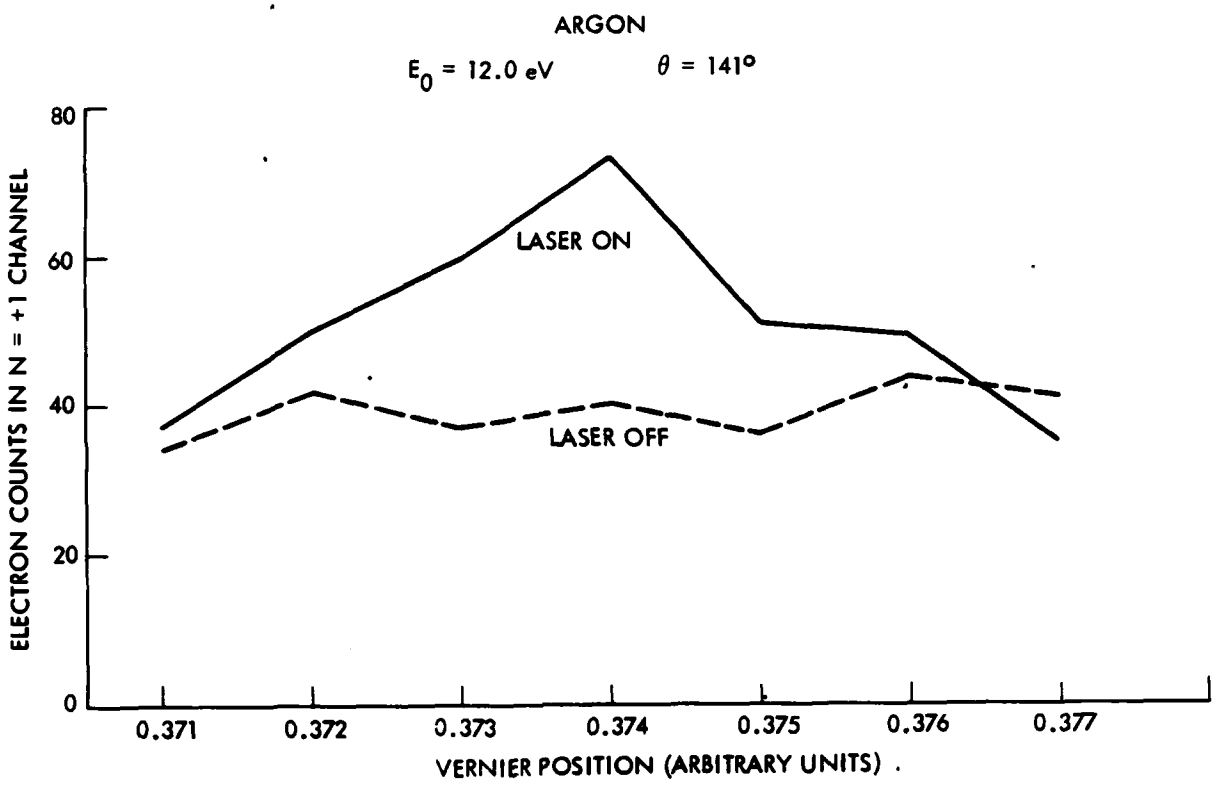

Figure 5.1. Measurement of the free-free signal as a function of laser position using the in plane geometry of Figure 4.5a. 4 minutes data accumulation per channel.

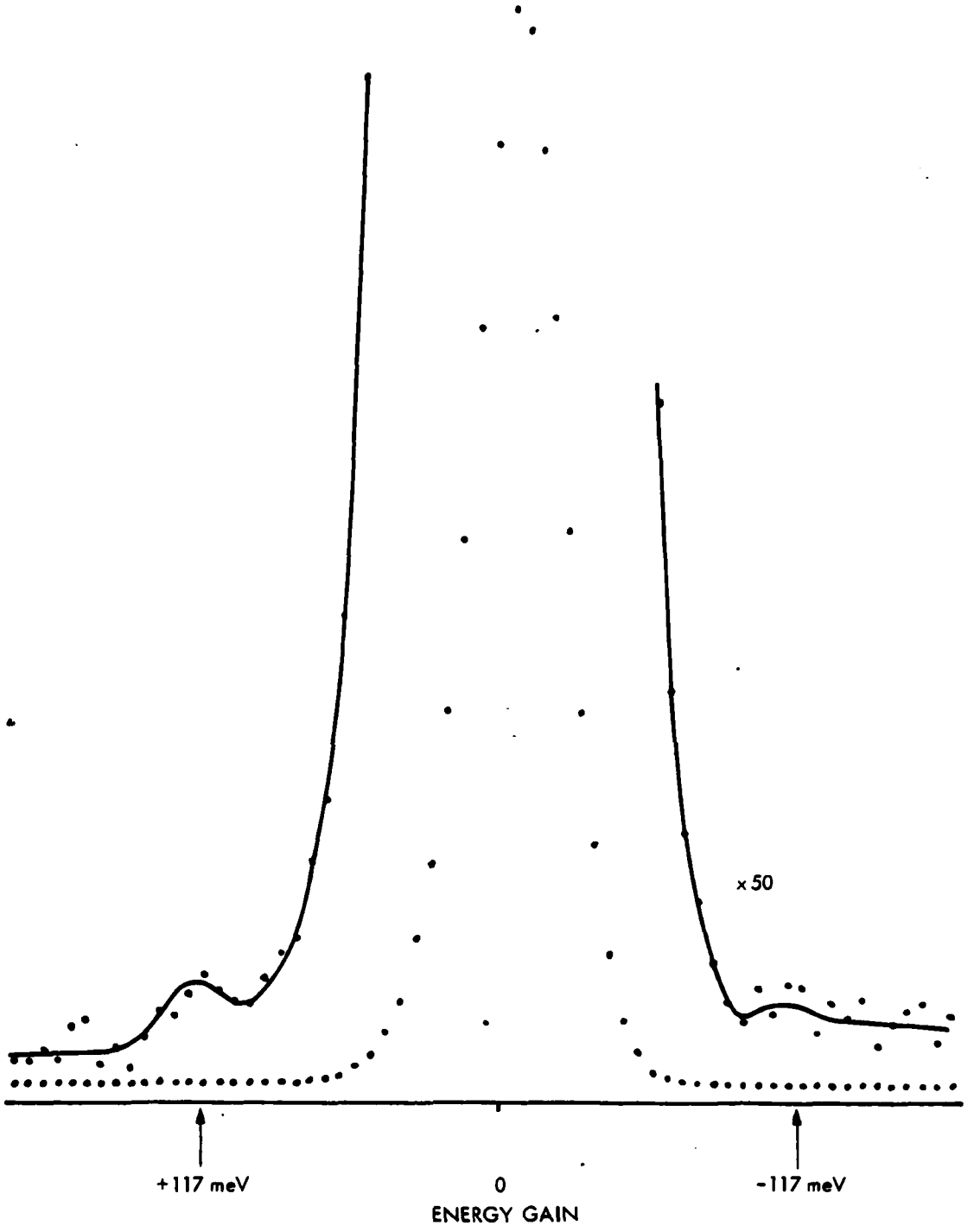

Figure 5.2. Energy spectrum of scattered electrons around the elastic peak.

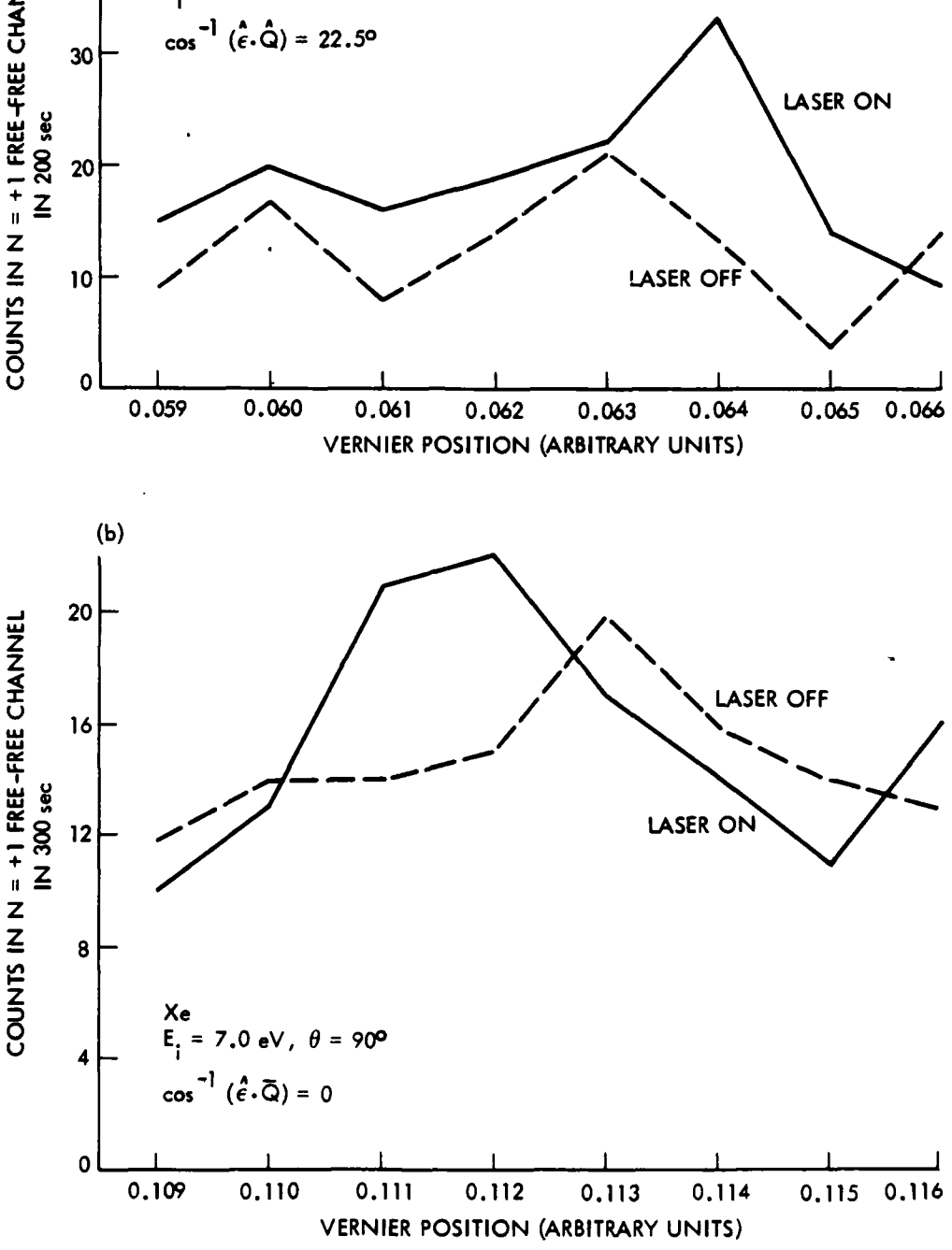

Figure 5.3. Measurement of the free-free signal as a function of the laser position using the geometry of Figure 4.5b.

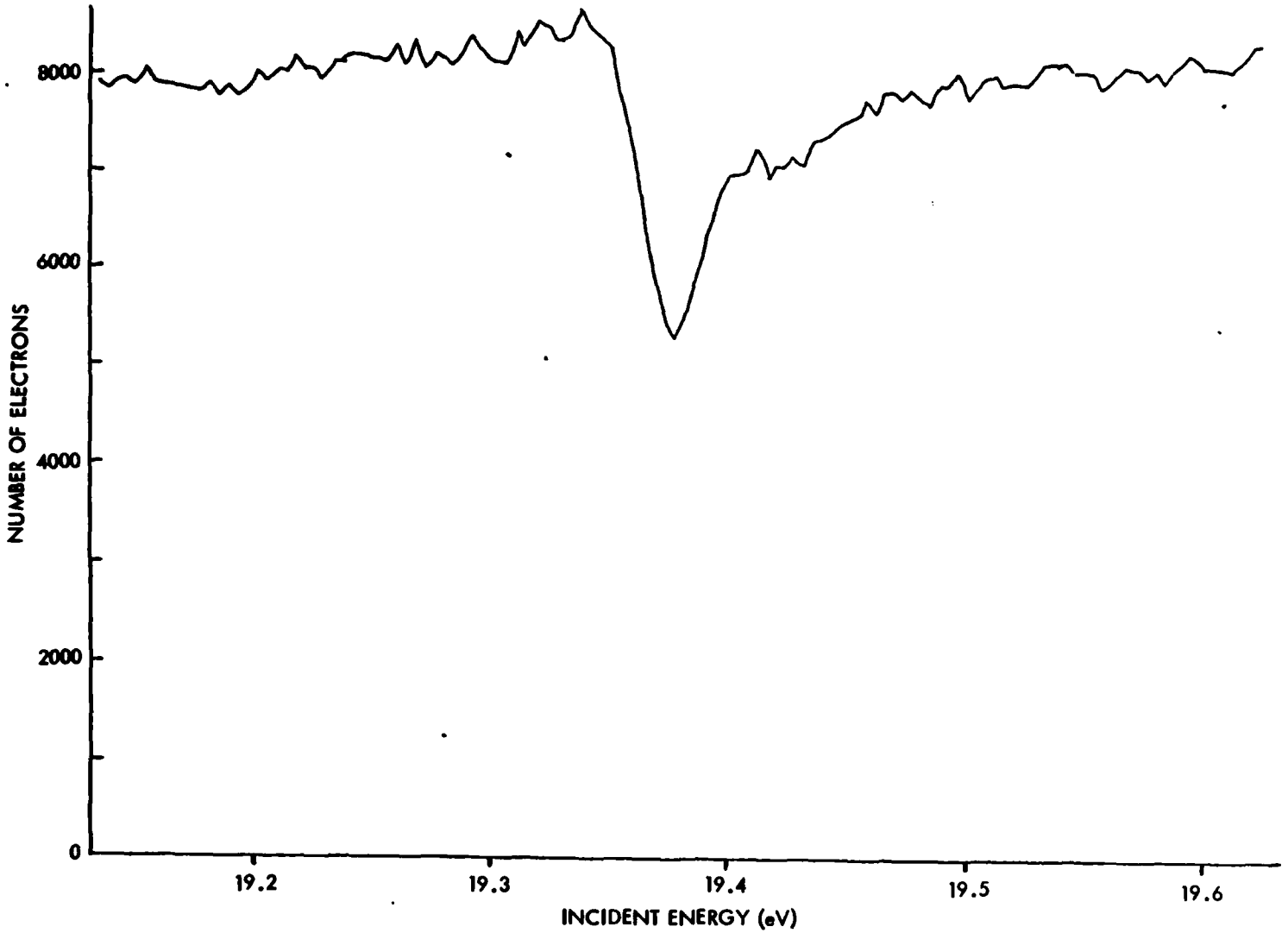

Figure 5.4a. He 2^2S resonance; $\theta = 141^\circ$

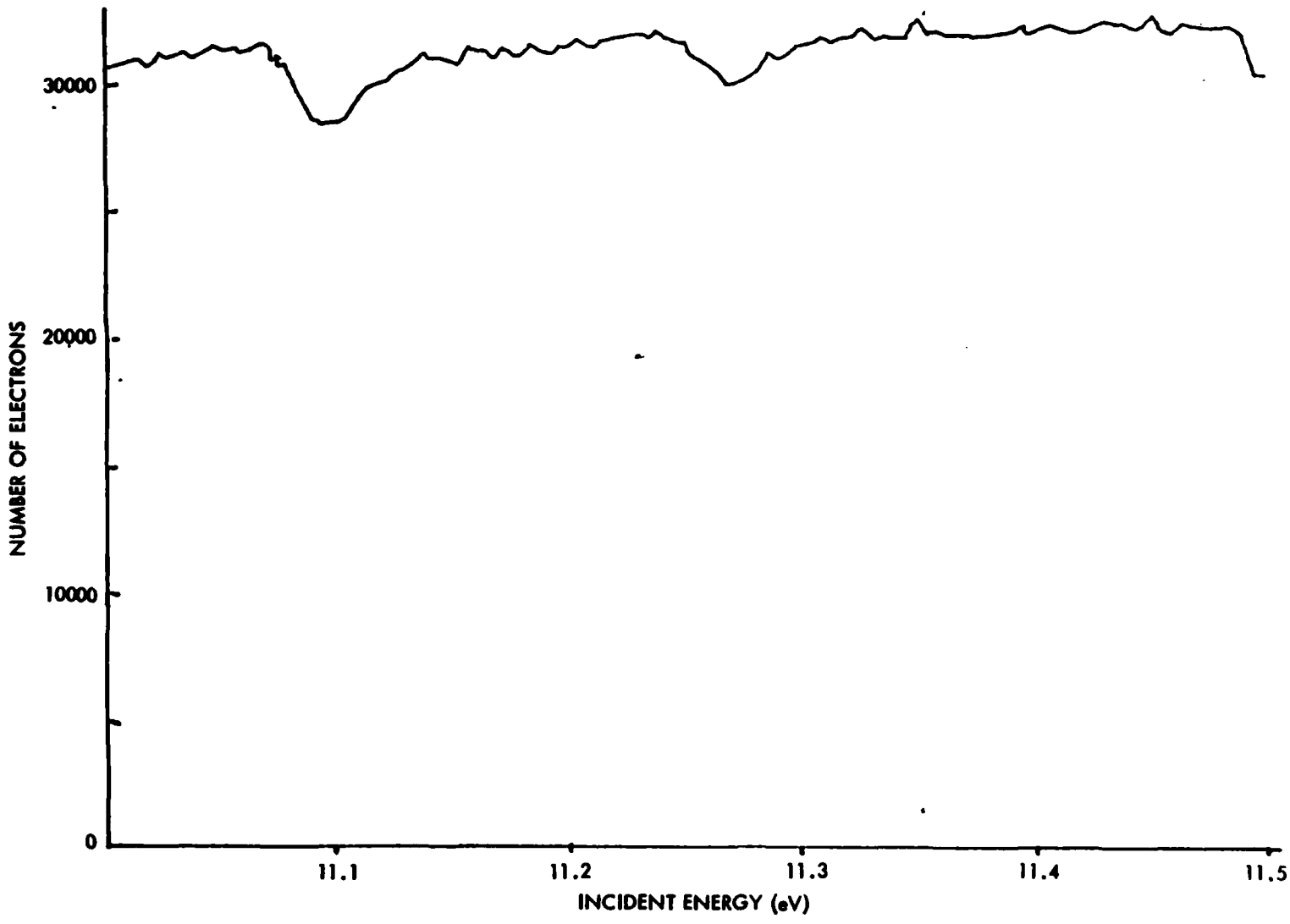

Figure 5.4b. Ar $^2P_{3/2}$, $^2P_{1/2}$ resonances; $\theta = 141^o$

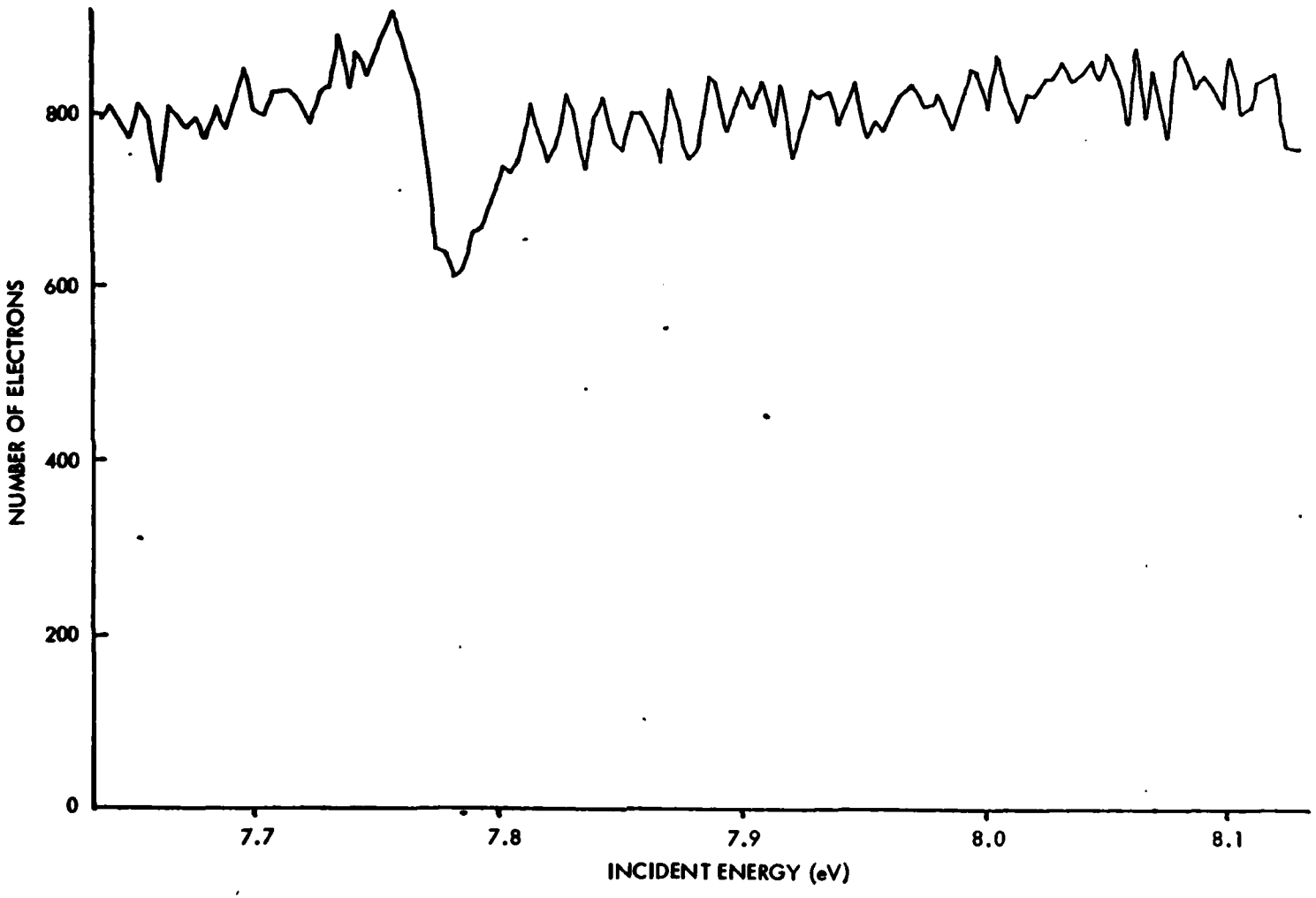

Figure 5.4c. Xe $^2P_{3/2}$ resonance; $\theta = 141^\circ$

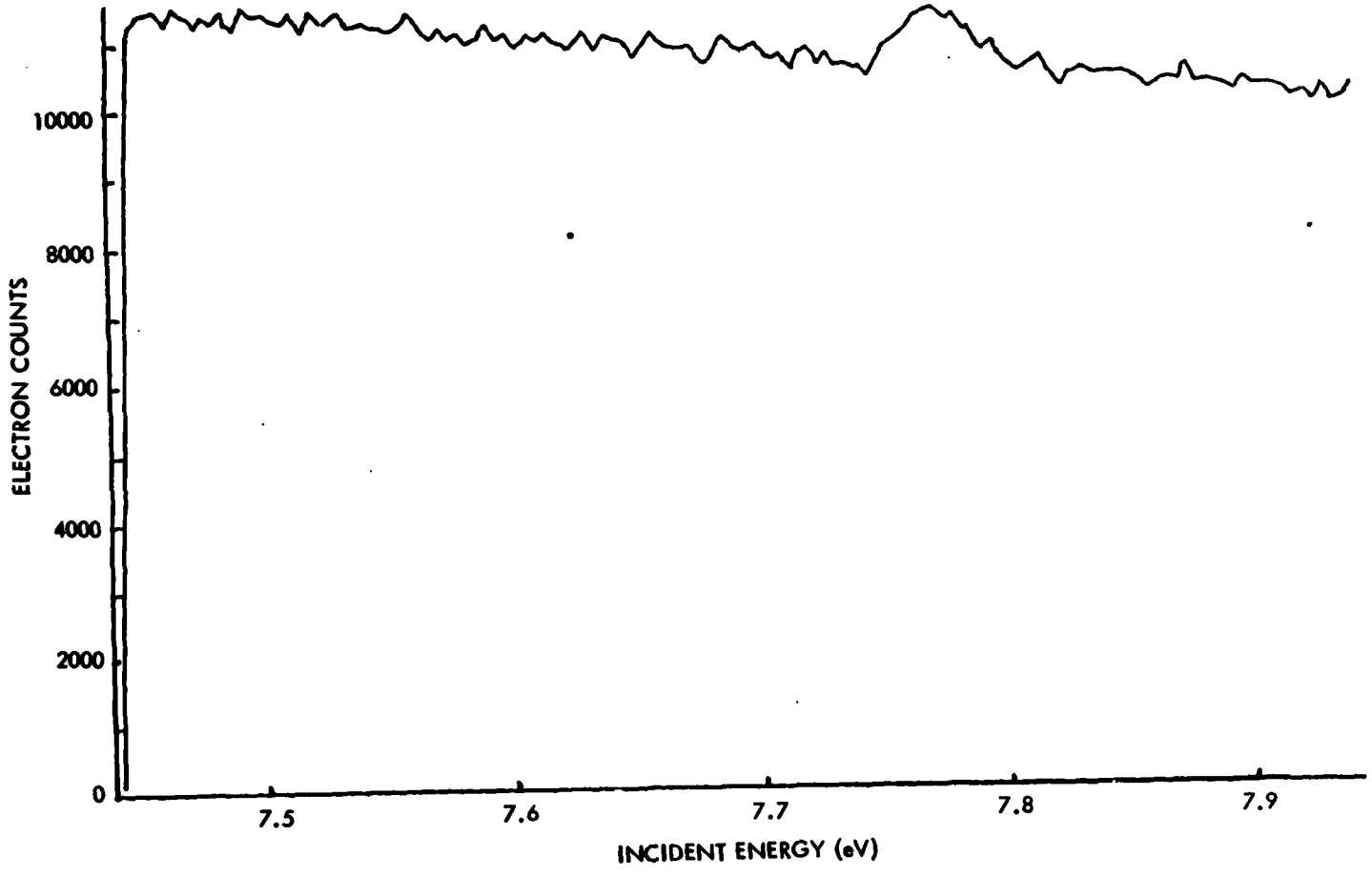

Figure 5.5. Xe $^2P_{3/2}$ resonance; $\theta = 90^o$

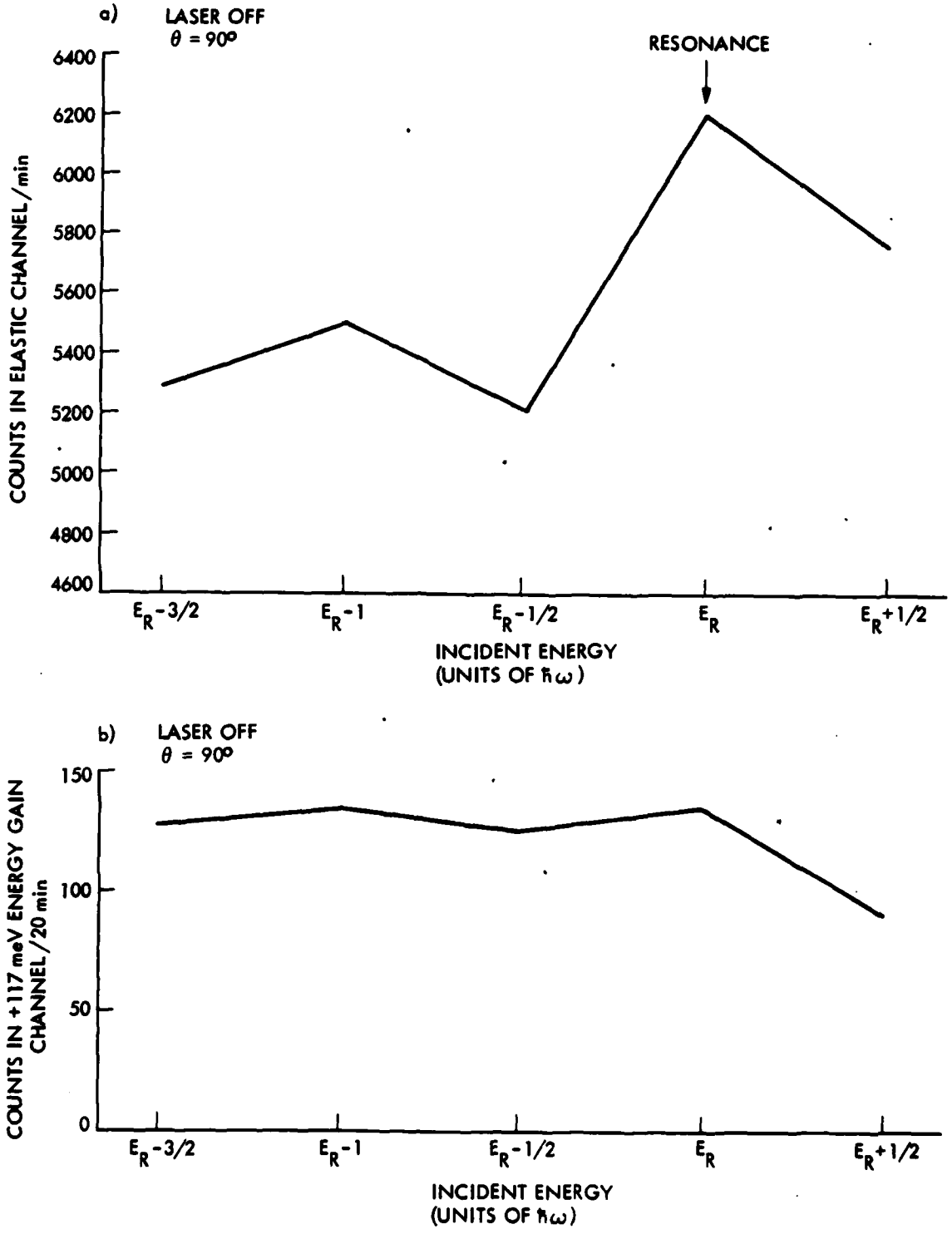

Figure 5.6. Scan of the Xe ($^2P_{3/2}$) resonance region: a, elastic channel; b, the +117 meV energy gain channel.

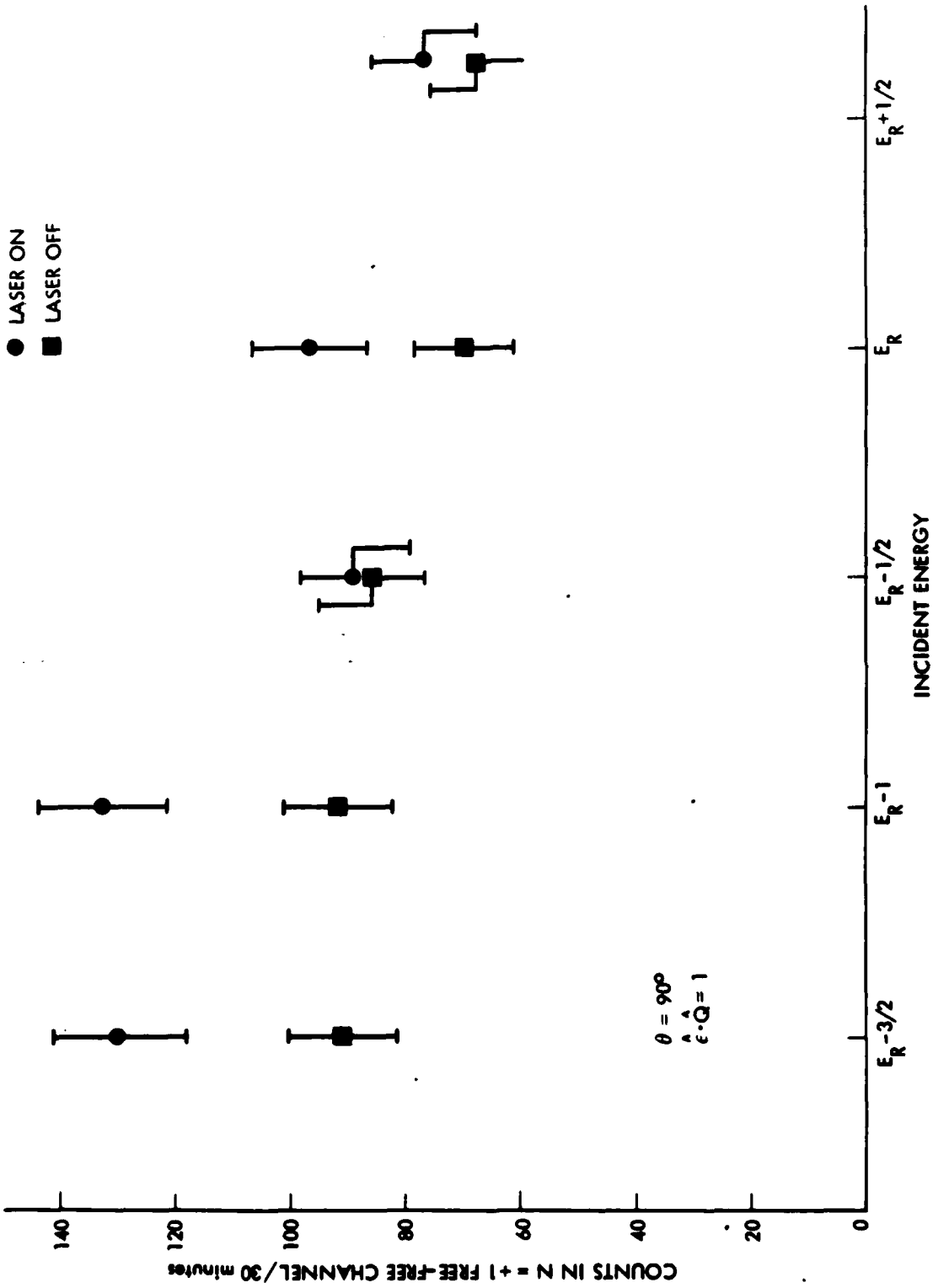

Figure 5.7. Counts in N = +1 free-free channel in the vicinity of Xe ($^2P_{3/2}$) resonance.

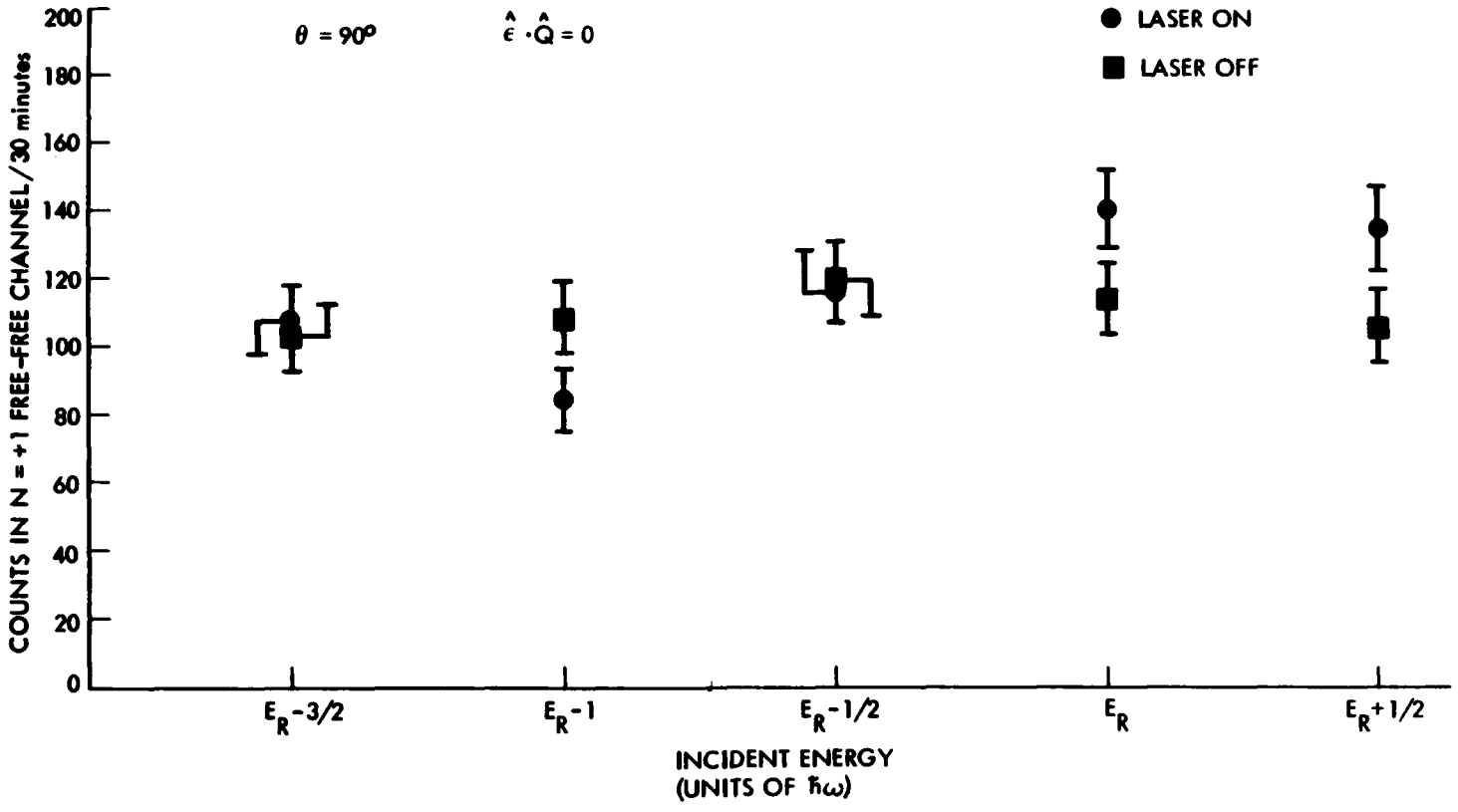

Figure 5.8. Counts in the N = +1 free-free channel in the vicinity of Xe ($^2P_{3/2}$) resonance

END

FILMED

4-85

DTIC